Mon. Not. R. Astron. Soc. **279**, 915–939 (1996)

Optical, infrared and millimetre-wave properties of Vega-like systems

R. J. Sylvester,[1] C. J. Skinner,[2★] M. J. Barlow[1] and V. Mannings[1†]

[1]*Department of Physics & Astronomy, University College London, Gower Street, London WC1E 6BT*
[2]*Institute of Geophysics & Planetary Physics, L-413, Lawrence Livermore National Laboratory, PO Box 808, Livermore, CA94551-9900, USA*

Accepted 1995 October 26. Received 1995 October 18; in original form 1995 August 10

ABSTRACT

Vega-like stars are main-sequence stars that exhibit excess infrared emission due to dust grains which are believed to be distributed in circumstellar discs. To facilitate modelling of the properties of the discs and of their constituent grains, we have assembled a new observational database for a large sample of candidate Vega-like systems, which comprises *UBVRI* optical photometry, *JHKLL'M* near-IR photometry, mid-IR spectra, and mm/submm-wave photometry.

Although our sample of stars are all believed to be main-sequence, it is noteworthy that most have large IR excesses compared with the 'prototype' Vega-like stars, and they may therefore be somewhat younger. The excess fluxes are, in a few cases, greater than can be explained by emission from pure radiation-reprocessing discs, even in the optically thick case, suggesting additional contributions by extended envelopes and/or flux generated by viscous dissipation in a flared accretion disc.

The dereddened optical colours are, for the whole sample, entirely consistent with photospheric emission from main-sequence stars. The near-IR photometry revealed that 9 out of 23 Vega-like sources exhibit excess near-IR emission with colours resembling those of Herbig Ae/Be systems, while the rest show only photospheric emission at near-IR wavelengths.

Our mid-IR spectra reveal that most of the discs show combinations of silicate and unidentified infrared (UIR) emission features, demonstrating the presence of both oxygen- and carbon-rich dust species. Our new mm/submm photometry indicates that most of the sample display small mm-wave spectral indices, implying that they possess grains that are much larger than those found in the interstellar medium, with implications for past or on-going grain growth within the discs.

Fractional excess luminosities, $L_{\rm IR}/L_{\star}$, were calculated from the optical photometry. For some of our sources, values $\sim 10^{-5} - 10^{-3}$ were found, similar to those of the prototype Vega-like systems. Others gave $L_{\rm IR}/L_{\star} > 0.25$, the maximum value for a flat passively reprocessing disc. Two sources gave $L_{\rm IR}/L_{\star} > 0.5$, the maximum for a flared reprocessing disc. These large values are comparable to those of Herbig Ae/Be and T Tauri stars, and suggest that some of the excess IR emission from these sources is due to disc accretion or the presence of circumstellar envelopes.

Key words: circumstellar matter – stars: evolution – planetary systems – infrared: stars.

1 INTRODUCTION

Vega-excess, or Vega-like, systems are main-sequence stars that exhibit profuse emission at far-IR wavelengths, with fluxes at $\lambda \gtrsim 60$ μm that can be more than an order of magnitude greater than those expected from the photospheres of stars of their spectral type. Such excess fluxes were found by Aumann et al. (1984) to be associated with the A0V star Vega (α Lyrae) following observations with the *Infrared Astronomical Satellite* (*IRAS*). The emission was attributed to a disc or ring of solid particles surrounding the star, possibly a remnant of a formerly massive disc, surviving from the era of formation of the star. A small group of bright stars, all resembling Vega in displaying

★ Present address: Space Telescope Science Institute, 3700 San Martin Drive, Baltimore, MD 21218, USA.
† Present address: California Institute of Technology, Department of Astronomy, 105–24 Pasadena, CA 91125, USA.

far-IR excesses, was soon identified from the *IRAS* survey data (Aumann 1985).

The largest far-IR excess amongst these prototypes was observed for the A5V star β Pictoris, for which Smith & Terrile (1984) presented *I*-band images showing light reflected from a greatly extended, nearly edge-on disc, hundreds of au in radius. Models of the reflected and thermally emitted radiation from this disc (Artymowicz, Burrows & Paresce 1989) suggest that the grains in the disc are principally in the size range from a few microns to a few tens of microns, which appears to be consistent with mm-wavelength photometry (Becklin & Zuckerman 1990). On the other hand, mid-IR spectra of β Pic (Telesco & Knacke 1991; Aitken et al. 1993; Knacke et al. 1993) revealed a silicate emission feature and indicated that the dominant emitting grain size at that wavelength is quite small, of the order of a micron.

The most recent optical images of the β Pic disc (e.g. Golimowski, Durrance & Clampin 1993) have been interpreted as implying that the grain composition may change suddenly beyond a radius corresponding to the sublimation temperature of water-ice. This could be analogous to conditions in the early solar nebula, which are thought to have allowed planetary cores formed in the outer Solar system to be very icy, while those that formed in the inner Solar system were principally rocky. A very comprehensive review of the observations of Vega-like systems, up to 1991, and the physical processes active in these systems, has been given by Backman & Paresce (1993).

It is clear that our Sun must once have had a very dusty disc around it, perhaps at one time similar to that surrounding β Pic. Following large-scale accretion of gas and dust on to the stellar surface during the pre-main-sequence phase of a star, a variety of processes should eventually deplete the disc remnant which may survive as the star arrives at the main sequence. These processes include

(i) Poynting-Robertson drag, which encourages small grains to fall on to the central star;

(ii) radiation pressure, which tends to drive grains in a range of sizes (depending on the spectral type of the star) out of the system altogether;

(iii) residual grain agglomeration and the final stages of planet-building.

These grain-depletion processes may occasionally be offset by the injection of new populations of dust particles resulting from collisions between larger- (e.g. asteroidal-) sized bodies. It might therefore be expected that main-sequence stars with a variety of spectral types and ages may possess discs with various grain size distributions and total masses.

To explore this hypothesis, we have compiled a set of observations of a large group of candidate Vega-like stars which have relatively large IR excesses. Some early results for several stars observed during this survey have already been published (Skinner, Barlow & Justtanont 1992; Skinner et al. 1995; Sylvester, Barlow & Skinner 1992, 1994b, 1996). In this paper we present the results of observations of our entire sample, from optical to mm wavelengths, together with some preliminary conclusions. In Section 2 we describe the selection of our sample of Vega-like stars. New observations made in the optical, infrared and mm-wave spectral regions are described in Section 3, and the results of these measurements are given in Section 4. Analyses of the data are described in Sections 4 and 5, and our conclusions are summarized in Section 6. Detailed radiative transfer models of the sources will be presented in a subsequent paper (Sylvester & Skinner, in preparation).

Table 1. Vega-like systems selected for multi-band observations. Spectral types either are from Dunkin, Barlow & Ryan (in preparation; henceforth DBR) or have been taken from the literature; see column 5 and the table footnote for references. An 'e' after the luminosity class indicates the presence of Hα in emission.

(1) Name	(2) HD	(3) SAO	(4) Spectral Type	(5) Ref[1].
49 Cet	9672	147886	A1V	1
35 Ari	16908	75532	B3V	2
HR 890	18537	23763	B7V	3
	23362	111388	K2	4
	23680	93601	G5	4
	34282	131926	A0	4
	34700	112630	G0V	9
	35187	77144	A2/3IV/V	9
HR 2522	49662	151962	B7IV	1
	98800	179815	K5V	10
Gl 471.2	109085	157345	F2V	1
	123160	158350	G5V	5
	135344	206462	F8Ve	6
	139614	226057	A7Ve	11
	141569	140789	A0Ve	12
	142666	183956	A8Ve	5
	142764	140845	K5	4
	143006	183986	G5Ve	13
	144432	184124	A9/F0Ve	14
HR 6398	155826	208591	G0V	7
51 Oph	158643	185470	A0Ve	1
	169142	186777	A4/5Ve	5
HR 8799	218396	91022	A5V	8
	233517	26804	K2	4

[1]References: **(1)** Michigan Spectral Survey, vol. 4 (Houk 1988); **(2)** Lesh (1968); **(3)** Murphy (1969); **(4)** Henry Draper Catalog; **(5)** DBR; **(6)** Coulson & Walther (1995); **(7)** Michigan Spectral Survey, vol. 3 (Houk 1982); **(8)** Welty et al. (1989); **(9)** Zuckerman, Forveille & Kastner (1995); **(10)** Upgren, Grossenbacher & Penhallow (1972); **(11)** Michigan Spectral Survey, vol. 2 (Houk 1978); **(12)** Andrillat, Jaschek & Jaschek (1990); **(13)** van der Veen et al. (1994).

2 SELECTION OF TARGET SOURCES

With the straightforward aim of maximizing our chances of determining grain and disc parameters, we selected those sources with the largest excess *IRAS* fluxes, i.e. we chose objects that were most likely to be detected over a wide range of wavelengths, and which were most likely to provide mid-IR spectra with good signal-to-noise ratio. Our sample comprises 24 sources in total, and they are listed by HD and SAO number in Table 1, together with their spectral types.

We excluded the four prototype Vega-like stars (Vega, β Pic, α PsA (Fomalhaut) and ε Eri) because they had already been observed in the submm region by Becklin & Zuckerman (1990) and by Chini, Krügel & Kreysa (1990) and Chini et al. (1991). β Pic, the only prototype with an excess at 12 μm, is too far south to be observed with the JCMT and UKIRT telescopes.

Various lists of Vega-like candidates have been published, e.g. Aumann et al. (1984), Aumann (1985), Gillett (1986), Sadakane & Nishida (1986), Stencel & Backman (1991). Perhaps the most useful is the list compiled by Walker & Wolstencroft (1988; henceforth WW), who selected objects according to the following criteria:

(i) association of positions of stars in the SAO catalogue with those of IR sources in the *IRAS* Point Source Catalog;
(ii) 60-μm/100-μm flux density ratios similar to those of the prototypes, i.e. between 0.8 and 2.0;
(iii) evidence for extended IR emission in one or more of the four *IRAS* photometric bands.

Objects were relegated by WW to a secondary list ('Section B') if (a) their available spectral classification contained an 'e', denoting the presence of emission lines; (b) they had a binary companion; (c) they had spectral classes indicating that they are late-type giants or supergiants.

We selected nine of the primary 'Section A' candidates listed by WW (SAO 26804, 77144, 112630, 147886, 183956, 184124, 186777, 206462, 226057), and three from the secondary list (SAO 179815, 140789 and 183986). We rejected some of the remaining sources because they were either M-class stars or cool giants/supergiants, and so were likely to be losing mass and producing dust of their own. Other sources were omitted simply because they are too far south to be observable from the observatories in Hawaii. We also selected one star, SAO 208591, from the WW list of associations with the Gliese (1969) catalogue which meet the first two of the above criteria but which were not required to show extension. SAO 208591 is the only star in that list that appeared to show large excesses in the *IRAS* bands: our observations (Section 4.3) indicate that this association is not correct.

Stencel & Backman (1991) published the results of a survey for IR excess emission in a flux-limited sample of stars, which was not limited to main-sequence stars, but also included evolved stars. They required that stars meet the following criteria.

(i) They must have a measured flux density at 12 μm, and in one or more of the longer-wavelength *IRAS* bands.
(ii) They must have a high galactic latitude, $|b| > 25°$.
(iii) The *IRAS* source must be positionally associated with an SAO star of spectral type B–M.
(iv) They must show excess emission in at least one of the *IRAS* 25-, 60- and 100-μm bands, compared with the 12-μm band flux. The 12-μm flux was (conservatively) assumed to be photospheric in origin.

This produced 379 stars with excess emission, out of a total of 5706 stars which satisfied criteria (i)–(iv) above.

We selected seven of these stars (SAO 75532, 91022, 93601, 111388, 131926, 140845, 158350), with spectral types B–K, and luminosity class V (if known). However, only one of these sources (SAO 131926) was detected at $\lambda = 1.1$ mm.

Three stars not listed by Walker & Wolstencroft or Stencel & Backman were also included. HR 890 (SAO 23763) and HR 2522 (SAO 151962) are included in the Backman & Paresce (1993) list of main-sequence Bright Star Catalog stars having IR excesses, while SAO 185470 (51 Oph) had been suggested to be a Vega-like star by Waters, Coté & Geballe (1988). None of these three stars was detected in our 1.1-mm JCMT observations.

A number of our stars lie close to 16 h RA, while a second group lies at approximately 5 h; interestingly close to the Scorpius–Ophiuchus and Orion star-formation regions respectively. The Vega-like stars may be young stars that have escaped from the star-formation regions, or possibly older stars that have passed through an interstellar cloud in those regions. Such a passage could, according to Whitmire, Matese & Whitman (1992), cause fragmentation of solid material in a previously existing circumstellar disc, which by increasing the population of small grains could enhance the IR excess of the star. Detailed studies of the proper motions and radial velocities of these Vega-like stars are needed to determine if either of the above scenarios is relevant to the present sample.

3 OBSERVATIONS

We have observed our sample of Vega-like stars at wavelengths in the optical, IR and mm-wave regions. Each wavelength régime is complementary in that it provides physical information that cannot be gleaned from the other observations. In addition to their individual contributions, our new data, when assembled together with *IRAS* measurements, define the optical–mm spectral energy distribution (SED) of each source, against which the results of new modelling can be compared.

For any given system, multi-band optical photometry enables the stellar photospheric contribution to the observed flux to be defined at all wavelengths since, given a spectral type, a suitable model atmosphere can be selected. Tabulated values of intrinsic colours versus spectral type then allow the reddening towards a star to be derived and the model atmosphere to be normalized to the dereddened optical fluxes. The normalized model atmosphere then provides a baseline for discrimination between normal and excess emission at longer wavelengths.

Photospheric fluxes can also be determined using near-IR photometry. In addition, such measurements define the short-wavelength limit of any excess emission, which can be produced by the hottest components of the circumstellar material.

Mid-IR 10- and 20-μm spectroscopy also allows the identification of the composition of circumstellar dust, since several of the most common constituent materials of grains have well-known mid-IR spectral features. Thus silicates display peaks in emission or absorption at wavelengths of 9.7 and 18 μm, while silicon carbide has a broad peak centred near 11.2 μm. In addition, the so-called 'unidentified infrared' (UIR) emission bands at 7.7, 8.7, 11.3 and 12.7 μm are believed to be associated with emission by carbonaceous species, such as polycyclic aromatic hydrocarbons (PAHs).

Finally, the *IRAS* far-IR fluxes and our new mm/submm photometry can be used to constrain the size of the largest grains present in a system, provided these grains are larger than a few microns in radius.

The new optical–mm photometric data for the present sample of sources are gathered together in Table 2, together with previously published photometry. The *IRAS* data for most of the stars was taken from the Point Source Catalog (PSC); the exceptions are SAO 147886, 93601 and 158350, where data in all four *IRAS* wavebands were taken from the Faint Source Survey Catalog (FSS), SAO 111388 and 91022, where the PSC 100-μm fluxes were taken but FSS fluxes were adopted for the other three wavebands, and SAO 140845,

Table 2. New and previously published optical–mm photometry. Columns 8 and 15 indicate the sources of optical and near-IR magnitudes; see the Table footnote for references. *IRAS* flux densities are taken mainly from the Point Source Catalog, with some from the Faint Source Survey Catalog; see text. Most of the mm/submm flux densities are new, with the exception of the 0.45-mm photometry for SAO 183956 and SAO 183986 (van der Veen et al. 1994), and the 0.45-mm point for SAO 206462 (Coulson & Walther 1995). All mm/submm upper limits are at the 3σ level.

(1) HD	(2) SAO	(3) *U* $\lambda(\mu m)$=0.38	(4) *B* (0.45μm)	(5) *V* (0.55)	(6) *R* (0.68)	(7) *I* (0.90)	(8) Ref	(9) *J* (1.22)	(10) *H* (1.65)	(11) *K* (2.18)	(12) *L* (3.55)	(13) *L'* (3.76)	(14) *M* (4.77)	(15) Ref	(16) F_{12} (Jy)	(17) F_{25} (Jy)	(18) F_{60} (Jy)	(19) F_{100} (Jy)	(20) 0.45 mm (mJy)	(21) 0.8 mm (mJy)	(22) 1.1 mm (mJy)	(23) 1.3 mm (mJy)	(24) 2.0mm (mJy)
9672	147886	5.78	5.70	5.61	–	–	1	5.54	5.51	5.51	5.53	–	5.51	2	0.34	0.38	2.02	1.88	–	–	–	–	–
16908	75532	3.91	4.54	4.67	4.69	4.82	3	4.91	4.94	5.00	5.05	–	5.06	2	0.41	<0.41	0.36:	<1.87	–	–	<39	–	–
18537	23763	4.76	5.18	5.23	–	–	4	5.37	5.38	5.41	5.43	–	5.46	2	0.53	0.68:	3.12:	14.08	–	–	<34	–	–
23362	111388	11.66	9.53	7.85	6.98	6.07	2	4.89	4.05	3.85	3.72	–	3.98	2	1.42	0.50	0.67	2.88	–	–	–	–	–
23680	93601	–	9.4	8.6	–	–	5	6.01	5.37	5.24	5.16	–	5.29	2	0.43	0.19	2.08	6.02	–	–	<45	–	–
34282	131926	10.16	10.05	9.88	9.79	9.68	2	9.02	8.20	7.44	6.53	–	–	2	0.70	1.63	10.80	10.72	1300±300	409±27	183±17	–	–
34700	112630	–	9.6	8.8	–	–	5	7.6:	7.8:	7.5:	7.0:	–	–	2	0.60	4.42	14.06	9.38	–	–	39±13	–	–
35187	77144	8.11	8.08	7.80	7.62	7.41	2	7.07	6.62	6.09	5.33	5.24	5.00	2	5.39	11.50	7.95	5.00	–	115±22	80±10	–	–
49662	151962	4.78	5.30	5.40	–	–	6	5.7:	5.5:	5.6:	5.8:	–	–	2	0.43	1.62	4.60	5.68	–	–	<42	–	–
98800	179815	11.26	10.14	8.89	8.12	7.38	7	6.44	5.82	5.66	–	–	5.5	8	1.98	9.28	7.28	4.46	<3600	111±12	63±6	11±3	–
109085	157345	4.71	4.69	4.32	3.94	3.76	3	3.69	3.57	3.54	3.51	3.55	3.59	2	2.24	0.77	0.31	0.80	–	–	–	–	–
123160	158350	12.20	10.12	8.62	7.81	6.94	2	5.86	5.07	4.87	4.73	4.76	5.33	2	0.62	0.37	3.11	4.41	–	<41	<16	–	–
135344	206462	9.14	9.14	8.63	8.16	7.83	9	7.31	6.67	5.97	–	4.89	4.54	9	1.59	6.71	25.61	25.69	<4500	570±21	209±14	142±19	<76
139614	226057	–	8.50	8.27	8.14	7.99	10	7.71	7.32	6.74	5.72	–	5.89	10	4.11	18.14	19.30	13.94	–	608±27	272±13	242±15	80±16
141569	140789	–	6.90	7.13	–	–	11	6.87	6.84	6.80	6.69	6.67	6.50	2	0.55	1.87	5.54	3.48	–	–	<36	–	–
142666	183956	9.35	9.20	8.65	8.36	7.98	2	7.32	6.70	6.02	5.04	4.95	4.85	2	8.57	11.21	7.23	5.46	1090±60	351±23	180±12	127±9	<63
142764	140845	–	10.7	9.3	–	–	5	6.41	5.58	5.35	5.20	5.21	5.49	2	0.37	0.11	<0.44	3.52	–	–	<45	–	–
143006	183986	11.30	11.02	10.18	9.73	9.22	2	8.35	7.65	7.06	6.14	6.06	6.18	2	0.86	3.16	6.57	4.82	1140±80	233±25	114±14	64±8	<132
144432	184124	8.65	8.50	8.17	7.93	7.71	2	7.16	6.57	5.95	5.00	4.91	4.52	2	7.53	9.36	5.77	3.29	–	103±34	69±10	–	–
155826	208591	6.61	6.54	5.96	–	–	12	4.93	4.64	4.58	4.55	4.59	4.52	2	3.67	5.35	8.63	<260	–	<220	<80	–	–
158643	185470	4.75	4.81	4.81	4.74	4.72	3	4.61	4.53	4.31	3.46	–	2.60	13	15.67	10.19	1.06	<5.97	–	–	<42	–	–
169142	186777	–	8.42	8.13	7.96	7.75	10	7.44	7.05	6.61	5.79	5.73	5.39	2	2.95	18.43	29.57	23.42	–	554±34	287±13	197±15	70±19
218396	91022	6.21	6.25	5.99	–	–	1	5.46	5.30	5.28	5.28	–	5.26	2	0.40	0.24	0.41	<2.59	–	–	<33	–	–
233517	26804	12.39	11.02	9.67	9.02	8.35	2	7.38	6.80	6.66	6.66	6.63	6.62	2	0.50	3.60	7.60	5.10	–	–	<36	–	–

References: **(1)** Cowley et al. (1969); **(2)** this paper; **(3)** Johnson et al. (1966); **(4)** Crawford, Barnes & Golson (1971); **(5)** SIMBAD database; **(6)** Lesh (1968); **(7)** Gregorio-Hetem et al. (1992); **(8)** Garcia-Lario et al. (1990); **(9)** Coulson & Walther (1995); **(10)** van der Veen, Habing & Geballe (1989); **(11)** Lindroos (1985); **(12)** Mermilliod (1986); **(13)** Waters, Coté & Geballe (1988).

Table 3. Stars observed photometrically in the optical region. Catalogue numbers without prefixes are from the Landolt (1983, 1992) catalogues.

Date (UT)	Stars Observed	
1993 Dec 2,3	Targets	SAO 26804,SAO 111388, SAO 112630, SAO 131926
	Standards	HD 39402, Gl 239, 980653, 950134, 990358
1994 April 6	Targets	SAO 183956, SAO 183986
	Standards	108148, PG1323-086A
1994 May 26	Target	SAO 184124
	Standard	109Z747
1994 June 10	Target	SAO 158350
	Standard	HD 121968

where the 12- and 25-μm fluxes are from the FSS, and the 60- and 100-μm fluxes are from the PSC.

3.1 Optical photometry

Photometry in the *U, B, V, R,* and *I* bands was obtained for the stars SAO 26804, 111388, 112630, 131926, 158350, 183956 and 184124 at the 1.0-m Jacobus Kapteyn Telescope (JKT). No published optical photoelectric photometry was available for any of these stars. The observations were made as part of the JKT Service programme, between 1993 December and 1994 June (see Table 3 for details of the observations). The detector used was the EEV7 charge-coupled device. Because the stars were known to be fairly bright (*V* magnitudes were typically between 8 and 10), the telescope was de-focused slightly to avoid saturating the detector.

The new optical photometry obtained with the JKT was reduced using the IRAF package; standard data reduction procedures of bias subtraction, flat-fielding, etc., were followed. All observations were corrected for atmospheric extinction. The corrections were determined using a theoretical extinction curve, calculated for the atmosphere above La Palma (Argyle et al. 1988), together with the actual visual extinction measured by the Carlsberg Automated Meridian Circle for the nights of our observations, obtained from the RGO archive. No colour corrections were applied to the photometry.

Photometric standard stars were taken from the catalogues of Landolt (1983, 1992). For the nights where there were observations of several standards, we were able to assess the quality of the observations by calibrating the standards against each other and comparing the magnitudes found in this way with the values quoted in the JKT CCD Handbook (Argyle et al. 1988). These tests showed the photometric data to be of good quality, with typical deviations of less than a few hundredths of a magnitude. The derived optical magnitudes are listed in Table 2.

3.2 Near-IR photometry

Near-IR photometry was obtained in the *J, H, K, L, L'* and *M* bands for a total of 16 of our sources using the single-channel bolometer UKT9 at the United Kingdom Infrared Telescope (UKIRT). Some of the observations were made by the authors in PATT time (1992 June 12, Table 4), the rest as part of the UKIRT Service programme. Circular apertures of 5 and 7.8 arcsec were used, and the telescope secondary was chopped at 3.5 Hz to enable background subtraction. Several different standard stars, selected from the UKIRT list, were observed on each night. A log of the UKT9 observations is given in Table 4.

Imaging photometry was obtained on 1993 September 17 and 18 using the UKIRT near-IR camera IRCAM (McLean et al. 1986), which employed a 58×62 element InSb array. The pixel scale was 0.62 arcsec per pixel. Eight Vega-like sources were observed, only three of which did not already have UKT9 near-IR photometry.

Reduction of the new UKT9 data was performed by the automated facility at the Joint Astronomy Centre (Hilo, Hawaii). Magnitudes were converted into flux densities using the isophotal wavelengths and flux calibrations of Cohen et al. (1992a), who define Vega to be zero magnitude at all infrared wavelengths shortwards of 20 μm. The derived near-IR magnitudes are listed in Table 2.

IRCAM observations of eight Vega-like systems were made on 1993 September 17 and 18; only three of these sources (see below) did not already have UKT9 near-IR photometry. Using observations of standard stars and previously observed Vega-like stars, we determined that September 18 was not a suitable night for photometry in the near-IR, so the magnitudes of SAO 112630 and HR 2522, indicated by colons in Table 2, should be treated with caution, although the data are good enough to give an indication that neither of these two stars shows a near-IR excess. The September 17 data are of higher quality, and the SAO 131926 magnitudes should be reliable.

3.3 Mid-IR spectroscopy

We obtained mid-IR spectra in the 10- and 20-μm bands for 13 of our sources (Table 5) in the course of three observing runs at UKIRT. The instrument used was the Cooled Grating Spectrometer 3 (CGS3), a common-user spectrometer designed and built at University College London, and commissioned in 1990 July. CGS3 contains three permanently mounted diffraction gratings, cooled using liquid helium to 4.2 K. Two of the three available gratings were used for these observations, namely the low-resolution 10- and 20-μm region gratings, which give spectral resolutions of 0.17 μm and 0.27 μm, respectively.

To sample fully the observed spectrum, two subspectra were taken with the grating positions displaced by half a resolution element. The subspectra were then interleaved in the data reduction process to produce a fully sampled 64-point spectrum. For our observations, the telescope secondary mirror was chopped east–west at 5 Hz with a 30-arcsec throw. Sky spectra taken using a rotating sector chopper were used for flat-fielding all spectra. The observed wavelength ranges were 7.5–13.5 μm and 15.8–23.9 μm. Wavelength calibration was with respect to a Kr arc lamp. A log of the CGS3 observations, with the standard stars used and the integration time per spectral point, is presented in Table 5. Allowing for the fact that two subspectra were taken for each spectrum, and for the overheads associated with chopping and nodding, the total observing time per spectrum was approximately 5.2 times the integration time per spectral point listed in Table 5.

The observed CGS3 spectra are presented in Fig. 1, along with colour-corrected *IRAS* flux densities at 12 and 25 μm. The colour corrections made to the *IRAS* photometry employed the energy distributions revealed by the CGS3 spectra,

Table 4. Log of UKT9 observations.

Date (UT)	Stars Observed		Aperture
1992 June 12	Targets	SAO 140789, SAO 140845, SAO 158350, SAO 183956, SAO 183986, SAO 184124, SAO 186777, SAO 208591, Gl 471.2	7.8 arcsec (*J–L'*), 5.0 arcsec (*M*)
	Standards	HD 161903, BS 6147, Y 4338	
1993 Feb 10	Targets	SAO 26804, SAO 77144	7.8 arcsec
	Standards	BS 2228, BS 3888, Gl 390	
1993 Sep 15	Targets	SAO 75532, SAO 91022, SAO 93601, SAO 111388, SAO 147886, HR 890	5.0 arcsec
	Standards	HD 3029, HD 18881, HD 162208, HD 163754, HD 2019141, HD 203856, BS 718, BS 1140, BS 8551	

Table 5. Log of CGS3 observations.

HD	SAO	Date (UT)		Standard		t_{int} (s)	
		10 μm	20 μm	10 μm	20 μm	10 μm	20 μm
35187	77144	31/10/93	–	α CMa	–	120	–
98800	179815	29,30/5/93	30/5/93	α Boo	σ Lib	750	400
123160	158350	1/6/93	–	α Boo	–	600	–
135344	206462	1/6/93	29/5/93	σ Lib	α Boo	510	600
141569	140789	1/6/93	30/5/93	σ Lib	α Boo	550	600
142666	183956	29/5/93	30/5/93	η Sgr	σ Lib	300	400
142764	140845	1/6/93	–	σ Lib	–	360	–
143006	183986	1/6/93	–	σ Lib	–	600	–
144432	184124	29/5/93	30/5/93	η Sgr	η Sgr	250	420
155826	208591	1/6/93	30/5/93	σ Lib	–	400	160
158643	185470	29/5/93	29/5/93	α Boo	α Boo	260	300
169142	186777	7/10/92	29/5/93	β Peg	β Peg	450	350
233517	26804	1/6/93	31/5/93	μ UMa	α Boo	700	350

together with the correction formulae defined by the *IRAS* Explanatory Supplement.

Each of the spectra was flux-calibrated by dividing the observed spectrum of a target source by that of a standard star, then multiplying by a model spectrum of the standard. Six standard stars were used, α Boo, α CMa, β Peg, σ Lib, η Sgr, and μ UMa. For α Boo, α CMa and β Peg, we used absolutely calibrated IR spectra provided by Dr M. Cohen, constructed in a similar way to the spectrum of α Tau described by Cohen, Walker & Witteborn (1992b). The other standards, σ Lib, η Sgr, and μ UMa, were assumed to emit as blackbodies with effective temperatures of 3640 K, 3600 K and 3895 K, and 10.0-μm fluxes of 188.6 Jy, 208.7 Jy and 99.0 Jy respectively.

Ratioing the target spectrum with that of a standard star during the data reduction process removes most of the artefacts due to telluric absorption, but often some data points remain contaminated. The spectral points most badly affected by atmospheric absorption have been discarded, hence most of the presented spectra contain fewer than 64 points in either band (10 or 20 μm). The discarded points tend to lie at approximately 9.5 μm, where there is a strong telluric ozone emission band, and at the edges of the atmospheric windows, where the atmospheric absorption is strongest. It is difficult to correct for the very heavy atmospheric absorption suffered by these points unless the spectra of both object and standard have very high signal-to-noise ratios.

Also plotted in Fig. 1 are the estimated mid-IR photospheric energy distributions, based on Kurucz model atmospheres normalized to the optical/near-IR photometry (see also Section 4.1). For some of the sources, e.g. SAO 183956 or SAO 184124, the photospheric contribution to the mid-IR flux is negligible compared with the excess emission; the dashed line representing the photospheric flux is barely visible above the abscissa, which represents zero flux. Conversely, for others, such as SAO 158350 or SAO 140845, there is no measurable excess in the 8–13 μm region, and the observed spectrum closely follows the predicted photospheric spectrum. This lends extra credibility to both the absolute flux calibration of the CGS3 spectra, and the photospheric spectra predicted using the model atmospheres.

Further confirmation of the accuracy of the absolute flux calibration of the CGS3 spectra is provided by the excellent agreement with the *IRAS* PSC 12-μm flux in almost all cases, independent of the shape of the mid-IR spectra and the level of excess emission.

The most notable exception is SAO 208591, for which the *IRAS* 12-μm flux is a factor of 5.5 higher than the CGS3 flux at 12.0 μm. This discrepancy is far too large to be due to inaccurate colour correction, so another explanation must be found. Pointing errors can be ruled out, as the star has an accurate SAO position and is optically bright ($V = 5.96$), and could easily be seen on the monitor screen of the UKIRT autoguider

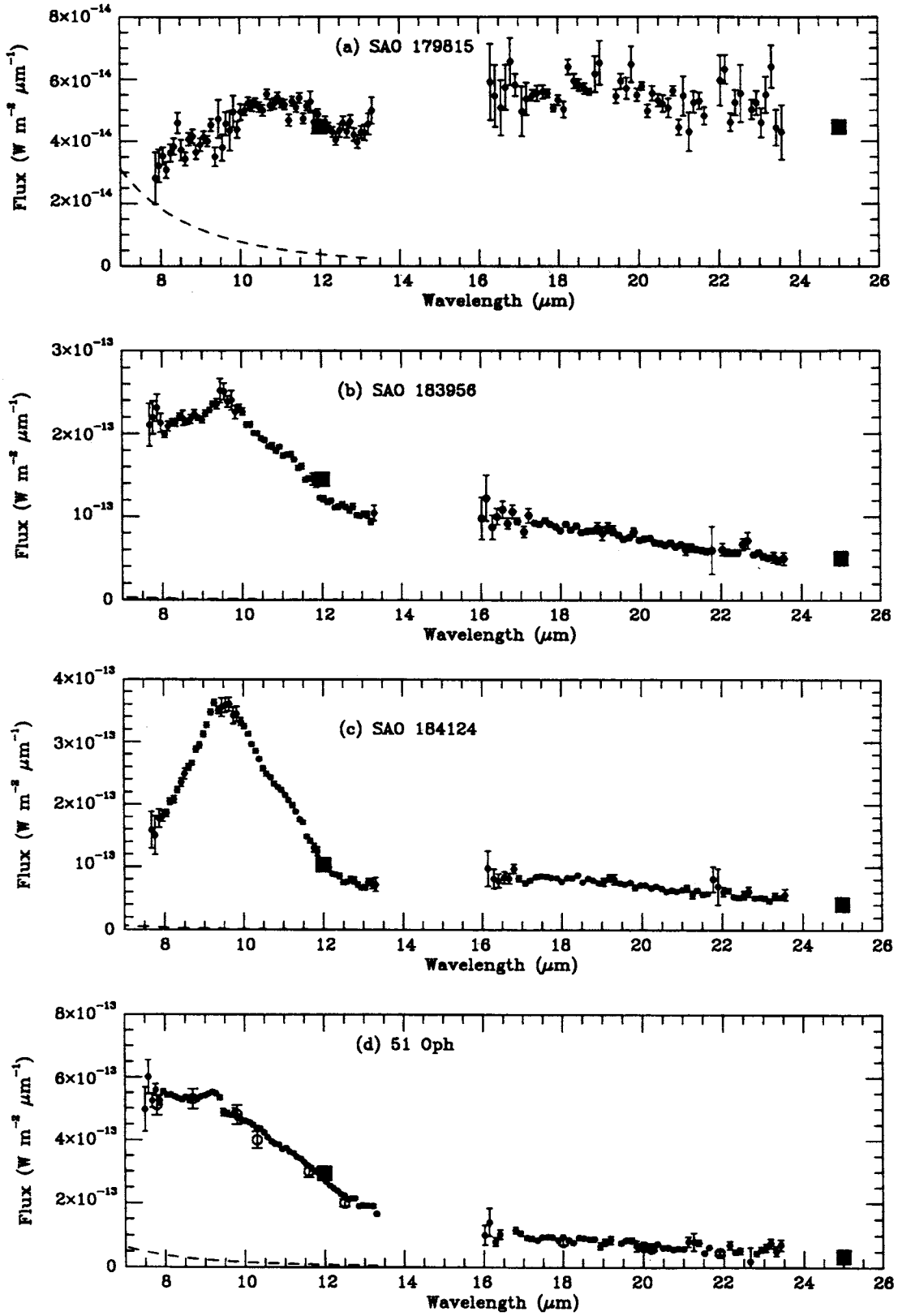

Figure 1. CGS3 10- and 20-μm spectra of Vega-like stars. Points with error bars: observed spectrum; filled squares: *IRAS* data; dashed line: model atmosphere (see text).

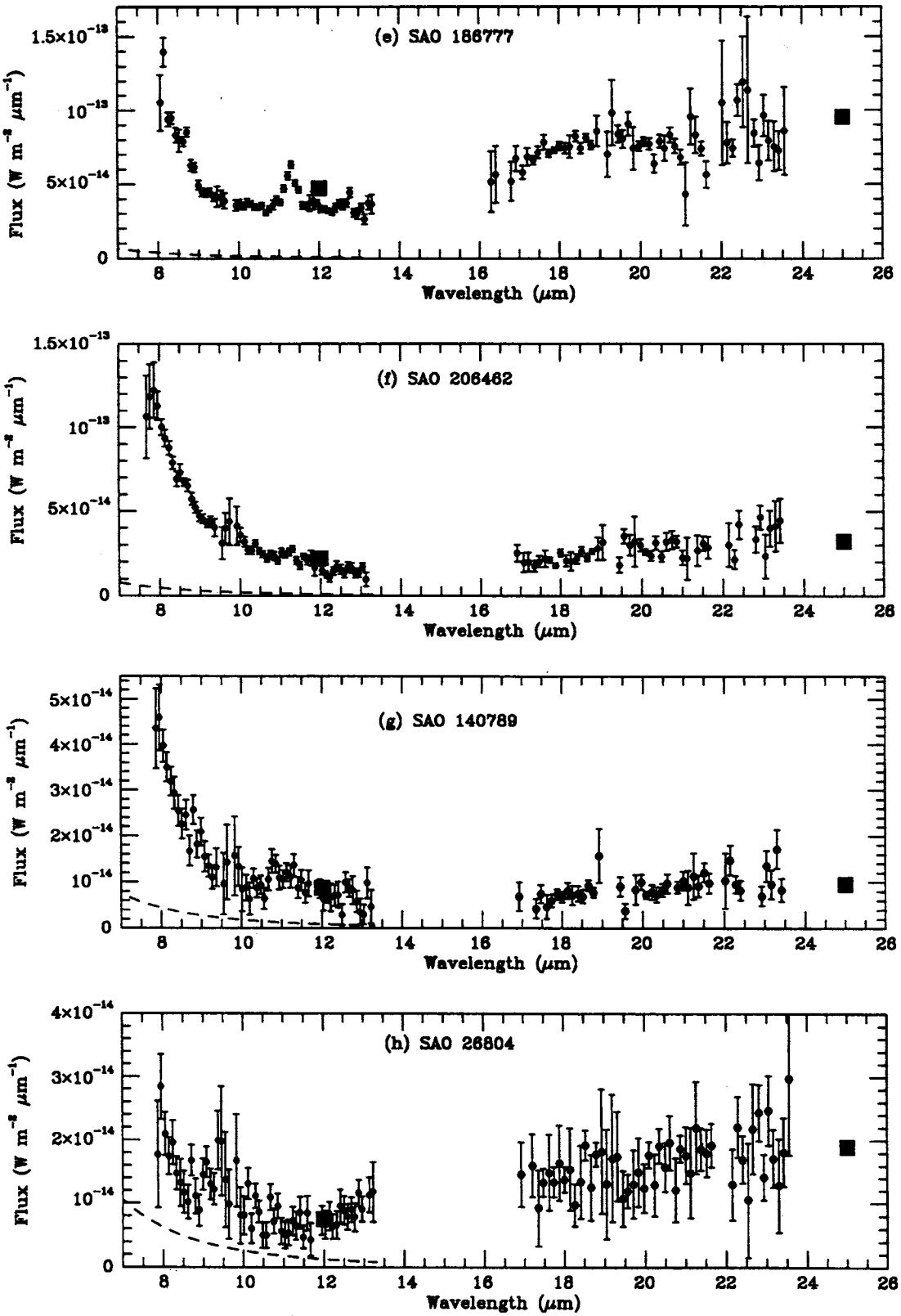

Figure 1 – *continued*

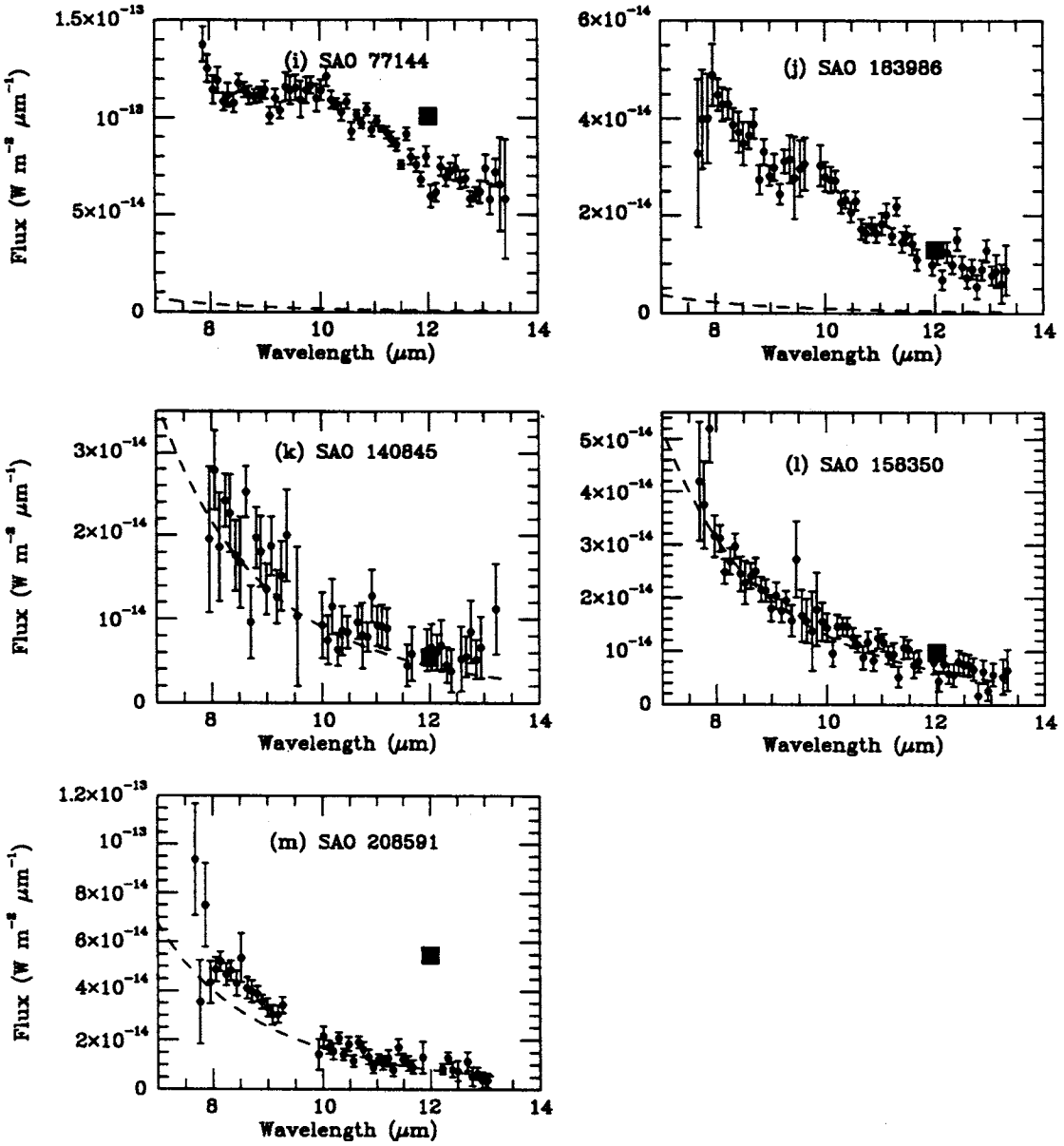

Figure 1 – *continued*

camera. There were no problems with the pointing behaviour of UKIRT for the other sources observed the same night.

The 10–13 μm portion of the CGS3 spectrum gives good agreement, in terms of both shape and overall flux level, with the predicted photospheric spectrum, so it seems that the observed 10-μm spectrum accurately represents the emission from SAO 208591. We also attempted to take a 20-μm spectrum of this source, but failed to detect it. The 3σ upper limits obtained for flux densities in the 16–23 μm band are all less than the *IRAS* 25-μm flux density (by a factor of $\sim$3), but are consistent with emission from the stellar photosphere.

The most reasonable explanation, therefore, is that the larger *IRAS* beam detected emission from other sources as well as SAO 208591, which did not appear in the 5.5-arcsec CGS3 beam. The location of SAO 208591 close to the Galactic plane, in the direction of the Galactic bulge (co-ordinates $l = 348°.5$, $b = -0°.1$), supports this argument, since this region of the Galactic plane is densely populated with IR sources. The position of SAO 208591 given in the SAO catalogue, with proper motion included up to 1983.0, is $\alpha = 17^h12^m10^s.4$, $\delta = -38°32'11''.1$ (1950 coordinates), while the position of the *IRAS* source is $\alpha = 17^h12^m09^s.5$, $\delta = -38°32'23''$. The discrepancy is larger than the CGS3 beamsize, but smaller than the *IRAS* beam, so it is quite possible that the *IRAS* source is physically distinct from SAO 208591. Examination of the *IRAS* Sky Survey Atlas image for the region around SAO 208591 shows significant Galactic emission at 12 μm, of which the supposed SAO 208591 emission appears to form a part.

3.4 Millimetre-wave photometry

Millimetre- and submm-wave photometry was obtained with the single-channel continuum receiver UKT14 at the James

Clerk Maxwell Telescope (JCMT) in 1992 February and August. We were allocated six eight-hour shifts at the telescope on both occasions, but lost some nights due to poor weather on each run. A third observing run took place in 1994 August, again under less than optimum weather conditions. Further data were kindly obtained for us by Dr I.D. Howarth in 1992 March, and in JCMT Service time in 1994 April and May.

UKT14 (Duncan et al. 1990) uses a single liquid-^{3}He-cooled bolometer and a set of filters ranging in nominal central wavelength from 0.35 mm to 2.0 mm. The observations presented here were made in the passbands centred nominally at 0.45, 0.8, 1.1, 1.3 and 2.0 mm. The UKT14 input aperture was kept at its maximum size for all our observations. This provided beamsizes of 18, 17, 19, and 21 arcsec for the 0.45-, 0.8-, 1.1- and 1.3-mm passbands, respectively.

Pointing- and focus-check observations were made at intervals throughout each observing shift. The pointing was found to be accurate to better than 3 arcsec. The telescope secondary was chopped at 7.8 Hz with a throw of 60 arcsec (90 arcsec for the 1992 February run) in azimuth, in order to remove the sky background.

We integrated for typically 10–30 min on our target sources. The noise equivalent flux density, calculated from the observations of calibration sources, was of the order of 0.5–2 Jy Hz$^{-1/2}$ at 1.1 mm, and 2–8 Jy Hz$^{-1/2}$ at 0.8 mm, compared with 0.7 and 5.0 quoted in the JCMT User Guide for a night with 'poor' atmospheric conditions. The weather conditions during the 1992 runs were very unstable, with the atmospheric opacity fluctuating markedly throughout each shift.

Frequent observations were made of standard sources (see below), typically more than 20 separate observations per night in a single waveband, chosen to give a good match to the programme sources in time and airmass. Pairs of standard observations, obtained at times bracketing the target observations, allowed the zenith optical depth and the instrument responsivity to be determined. Responsivities derived in this way are consistent with the values quoted in the JCMT Manual (Matthews 1993).

Weather conditions during the 1994 August run were slightly less troublesome. Atmospheric transmission measurements at 1.3 mm provided by the Caltech Submillimeter Observatory radiometer, located adjacent to the JCMT, indicated a poor but very stable zenith optical depth of about 0.2 at 1.3 mm during each of the four nights. Such stability allows a rough determination of the instrument responsivity and the optical depth of the atmospheric extinction using a linear least-squares fit to a secant plot for the observations of standard sources.

By way of comparison, a second calibration method was used, employing the empirical ratios of $\tau_\lambda/(\mathrm{CSO}\ \tau_{1.3\mathrm{mm}})$ determined by Stevens & Robson (1994) from observations made between 1992 and 1994, together with the calibration observations. The two methods were in good agreement. The average transmission at the zenith during each of the four shifts ranged from $\approx$ 35 per cent at 0.8 mm to $\approx$ 85 per cent at 2 mm. Little variation in sky opacity was observed between the four shifts of this run.

In the three observing runs reported here, the calibrators used were Mars, Uranus, and the secondary standards 16293−2422, 2251+158, 3C279, G343.0, G45.1, GL490, K-350, NGC2071IR and W75N, the fluxes and positions of which are all given in the list published by Sandell (1994).

Table 6. Individual JCMT measurements.

HD	SAO	Date	Filter (mm)	Flux (mJy)
16908	75532	1992 Aug	1.1	16±13
18537	23763	1992 Aug	1.1	<34
23680	93601	1992 Aug	1.1	33±15
34282	131926	1992 Aug	1.1	183±17
		1993 Dec	0.45	1318±254
		1993 Dec	0.8	409 ±27
34700	112630	1992 Aug	1.1	39±13
35187	77144	1992 Aug	1.1	80±10
		1993 Dec	0.8	115±22
49662	151962	1992 Aug	1.1	<42
98800	179815	1992 Feb	0.8	111 ±12
		1992 Feb	1.1	88±11
		1992 Mar	1.1	60±6
		1994 Apr	0.45	1234±1272
		1994 Apr	1.3	11±3
123160	158350	1992 Feb	0.8	<41
		1992 Feb	1.1	<47
		1992 Mar	1.1	<16
135344	206462	1992 Feb	0.8	570±21
		1992 Feb	1.1	209±14
		1994 Aug	1.3	142 ± 19
		1994 Aug	2.0	<76
139614	226057	1992 Feb	0.8	608±27
		1992 Feb	1.1	264±16
		1994 Aug	1.1	287±24
		1994 Aug	1.3	242±15
		1994 Aug	2.0	80±16
141569	140789	1992 Feb	1.1	<44
		1992 Mar	1.1	<36
142666	183956	1992 Feb	0.8	351±23
		1992 Feb	1.1	167±17
		1994 Apr	0.45	1022±315
		1994 Apr	1.3	118±15
		1994 Aug	0.8	< 795
		1994 Aug	1.1	190±17
		1994 Aug	1.3	131 ±11
		1994 Aug	2.0	<63
142764	140845	1992 Feb	1.1	<63
		1992 Aug	1.1	<45
143006	183986	1992 Feb	0.8	233±25
		1992 Feb	1.1	114±17
		1994 Apr	0.45	720±340
		1994 Apr	1.3	57±17
		1994 Aug	1.3	65±9
		1994 Aug	2.0	<132
144432	184124	1992 Feb	1.1	58±19
		1992 Aug	0.8	103±34
		1992 Aug	1.1	72±12
155826	208591	1992 Feb	0.8	<220
		1992 Feb	1.1	<80
		1992 Aug	1.1	31±17
158643	185470	1992 Aug	1.1	26±14
169142	186777	1992 Feb	0.8	504±48
		1992 Feb	1.1	302±19
		1992 Aug	0.8	606±49
		1992 Aug	1.1	271±19
		1992 Aug	1.3	197±15
		1992 Aug	2.0	<213
		1994 Aug	2.0	70±19
218396	91022	1992 Aug	1.1	28±11
233517	26804	1992 Mar	1.1	<36

Table 7. IRAM 1.2-mm fluxes (in mJy) of Vega-like stars from Bockelée-Morvan et al. (1995).

HD	SAO	1-channel	7-channel
9672	147886	12.7±2.3	–
18537	23763	–	3.8±1.5
98800	179815	59.1 ±5.4	26.5±3.1
142666	183956	161±5.5	78.6±5.4
144432	184124	61.4±5.3	41.9±0.4
158643	185470	–	<28.2
169142	186777	–	178.5±0.6
218396	91022	4.0±2.7	–

Table 8. The adopted zero-magnitude flux calibration for optical and near-IR photometry, taken from Deacon (1991).

Filter	λ_{iso} (μm)	F_λ W m^{-2} μm^{-1}
U	0.376	4.183×10^{-8}
B	0.453	6.239×10^{-8}
V	0.547	3.602×10^{-8}
R	0.680	1.869×10^{-8}
I	0.898	9.254×10^{-9}
J	1.215	3.314×10^{-9}
H	1.654	1.151×10^{-9}
K	2.179	4.139×10^{-10}
L	3.545	6.608×10^{-10}
L′	3.761	5.263×10^{-10}
M	4.769	2.107×10^{-10}

Note: λ_{iso} = isophotal wavelength, F_λ = flux density at zero magnitude.

The individual calibrated fluxes obtained are presented in Table 6. Where we made several separate observations of a given source using the same filter, we have computed the weighted mean flux density and uncertainty. The fluxes presented in Table 2 are, where appropriate, the weighted means of the observed flux densities from all the observing runs. The weighting factors used were the squares of the signal-to-noise ratios of the individual measurements.

We have 3σ or better detections of ten sources in at least one waveband (nine of these were detected in at least two bands), and upper limits on the 1.1-mm flux from a further eleven sources. (The 0.45-mm flux measurement for SAO 206462 – from Coulson & Walther 1995 – is at the 2.5σ level, but the corresponding 3σ upper limit has been entered in Table 2.)

Two of the sources observed at 1.1 mm in the 1994 August run, SAO 183956 and SAO 226057, had also been observed in the 1992 February run. There is good agreement between the two sets of measurements, which were calibrated using different methods, giving additional confidence in the calibrated fluxes. Results of the 1992 February and August observations of SAO 77144, 91022, 112630, 131926, 179815, 183956, 183986, 184124, 186777, 206462, and 226057 were published in Sylvester et al. (1994b).

Two Vega-like stars, SAO 183956 and SAO 183986, were observed with the JCMT in 1991 May by van der Veen et al. (1994). Observations of both stars were made at 0.45, 0.8 and 1.1 mm, using similar techniques to those described above. The fluxes measured by those authors for SAO 183956 were 1090±60 mJy, 287±10 mJy, and 145±12 mJy, at 0.45, 0.8 and 1.1 mm respectively, while those for SAO 183986 were 1140±80 mJy, 162±14 mJy, and 87±17 mJy at the same wavelengths. These are in reasonable agreement with our new values presented in Table 2, within approximately twice the formal error on the measurements.

Bockelée-Morvan et al. (1995) recently observed a number of Vega-like stars at 1.2 mm using the Institut de Radio Astronomie Millimétrique (IRAM) 30-m telescope. Observations were made in 1993 December using a single-channel bolometer, and in 1994 May using the MPIfR seven-channel bolometer array. The flux measurements with the two detectors are reproduced in Table 7. As can be seen from Table 7, there are significant differences between the fluxes obtained in the December and May runs. Bockelée-Morvan et al. ascribe these to difficulties in calibrating the May (seven-channel) data, which were obtained under poor atmospheric conditions.

We have JCMT measurements of three of the stars for which Bockelée-Morvan et al. obtained detections above the 3σ level with the single-channel bolometer: SAO 179815, 183956 and 184124. In all three cases, the Bockelée-Morvan et al. single-channel 1.2-mm measurements are in good agreement with the JCMT fluxes. For SAO 179815 and 183956, where we have JCMT data at 1.1 and 1.3 mm, the IRAM fluxes lie between the two JCMT values.

The IRAM beamwidth at 1.2 mm (10–12 arcsec) is about half that of the JCMT beam at 1.1 mm (19 arcsec). The close agreement between the fluxes measured by the two telescopes suggests that the mm-wave emitting regions of these three objects are not significantly extended with respect to the IRAM beam.

SAO 186777 was observed by Bockelée-Morvan et al. (1995) using only the seven-channel bolometer. The 1.2-mm flux they measured was roughly 50 per cent lower than would be expected from interpolation between our 1.1- and 1.3-mm JCMT measurements. However, this should not be taken as evidence of extension of this source with respect to the IRAM beam, since, for the three sources mentioned above (which had both one-channel and seven-channel detections), the seven-channel flux was of the order of 50 per cent lower than that measured with the single-channel detector, which gave results consistent with our JCMT data.

4 DERIVED PROPERTIES

4.1 Optical SEDs

Values of $(B-V)_0$ as a function of spectral type, taken from Schmidt-Kaler (1982), together with the observed $B-V$ colours, have been used to derive the reddening, $E(B-V)$, towards each star. The photometry was then dereddened using a 'standard' Galactic reddening law based on the fits of Seaton (1979) and Howarth (1983). The data were converted from magnitudes to flux densities using the flux calibration of Deacon (1991). The adopted zero-magnitude flux densities are presented in Table 8. The dereddened photometry could then be compared with Kurucz (1991) model atmosphere fluxes. The appropriate model atmospheres were selected using the Schmidt-Kaler (1982) calibration of T_{eff} and log g against

Table 9. Distances and reddenings derived from JKT service optical photometry.

HD	SAO	Sp. Type	$(B-V)$	$(B-V)_0$	m_V	E$(B-V)$	M_V	d(pc)
23362	111388	K2	1.68	0.91	7.85	0.77	6.4	6.5
34282	131926	A0	0.28	-0.02	9.88	0.19	0.6	547
35187	77144	A2/3 IV/V	0.17	0.05	7.80	0.23	1.3	202
123160	158350	G5V	1.50	0.68	8.62	0.82	5.1	15.7
142666	183956	A8Ve	0.56	0.25	8.65	0.31	2.4	114
143006	183986	G5Ve	0.84	0.68	10.18	0.16	5.1	82
144432	184124	A9/F0Ve	0.33	0.30	8.17	0.03	2.7	119
233517	26804	K2	1.35	0.91	9.67	0.44	6.4	28

Table 10. Distances and reddenings derived from published optical photometry.

HD	SAO	Sp. Type	$(B-V)$	$(B-V)_0$	m_V	E$(B-V)$	M_V	d(pc)
9672	147886	A1V	0.09	0.01	5.61	0.08	1.0	75
16908	75532	B3V	-0.13	-0.21	4.67	0.08	-1.6	160
18537	23763	B7V	-0.05	-0.14	5.23	0.09	-0.6	129
49662	151962	B7IV	-0.10	-0.14	5.40	0.04	-0.6	188
98800	179815	K5V	1.25	1.15	8.89	0.10	7.4	17
109085	157345	F2V	0.72	0.35	4.32	0.37	3.6	14
135344	206462	F8Ve	0.51	0.52	8.63	-0.01	4.0	84
139614	226057	A7Ve	0.23	0.20	8.27	0.03	2.2	157
155826	208591	G0V	0.58	0.58	5.96	0.00	4.4	21
158643	185470	A0Ve	0.00	-0.02	4.81	0.02	0.6	68
169142	186777	A4/5Ve	0.29	0.15	8.13	0.14	1.9	145
218396	91022	A5V	0.26	0.15	5.99	0.11	1.9	56

spectral type, together with the spectral types of the Vega-like stars given in Table 1.

Good agreement was found between the dereddened photometry and the model atmospheres, indicating that the stars do not deviate markedly from normal main-sequence stars at optical wavelengths and that abnormal reddening laws are not encountered.

Values of $E(B-V)$ are listed in Table 9, along with the distances to the stars derived from the new JKT photometry. Absolute magnitudes and intrinsic colours for the various spectral types were taken from Schmidt-Kaler (1982). The corresponding quantities for the stars with photoelectric photometry already available in the literature were also calculated, and are presented in Table 10.

The observations of SAO 111388 indicate that it is highly reddened and remarkably close, at 6.5 pc. No parallax data are available to confirm this result, but SAO 111388 is in the *Hipparcos* Input Catalogue (as number 17473), so a parallax measurement should be available in the near future. It is possible that the spectrum was misclassified in the HD catalogue, and is really of type M, and hence has redder intrinsic colours. If this were the case, however, the star would be even closer, since the effect of lower intrinsic luminosity (i.e. larger M_V) would outweigh that of a smaller amount of extinction.

SAO 77144 is a double star, with the two components having equal V magnitudes (Turon et al. 1992). The distance given in Table 9 was calculated assuming they are both of spectral type A2V.

The value of $E(B-V)$ obtained for SAO 206462 is actually slightly negative (−0.01) but, for the purposes of the distance calculations, was treated as zero. Since the accuracy of the photometry is of the order of 0.01 mag, the discrepancy can safely be neglected.

The fluxes corresponding to the dereddened photometric data are plotted in Fig. 2.

4.2 Near-IR SEDs

Comparing the observed near-IR fluxes with the Kurucz (1991) model atmospheres we see that, for the majority of our sources, there is good agreement between observed and predicted fluxes, demonstrating that, as expected, a normal stellar photosphere is the dominant source of near-IR flux. However, nine of our 23 sources show excess emission in one or more of the near-IR photometric bands, clearly discernible by inspecting the SEDs or by comparing the observed near-IR colours with their theoretical values (presented in Deacon 1991).

This cannot be due to an abnormal reddening law, since dereddening using the standard value of $R = A_V/E(B-V) = 3.1$ produces a very good match between optical photometry and the model atmosphere for all the sources. Attempts were made to deredden the SED of SAO 186777 using higher values of R, appropriate for the more nearly 'grey' extinction that would be caused by larger dust grains than those present in the interstellar medium. No reddening law, even for values of R as high as 10, was able to increase sufficiently the optical flux so as to remove, even approximately, the near-IR excess without at the same time giving $(U-B)$ and $(B-V)$ colours that were far too blue.

The magnitudes of the excesses in the various near-IR wavebands are presented in Table 11. They were calculated by fitting a Kurucz model atmosphere to the dereddened optical photometry, determining the ratio of the observed fluxes to

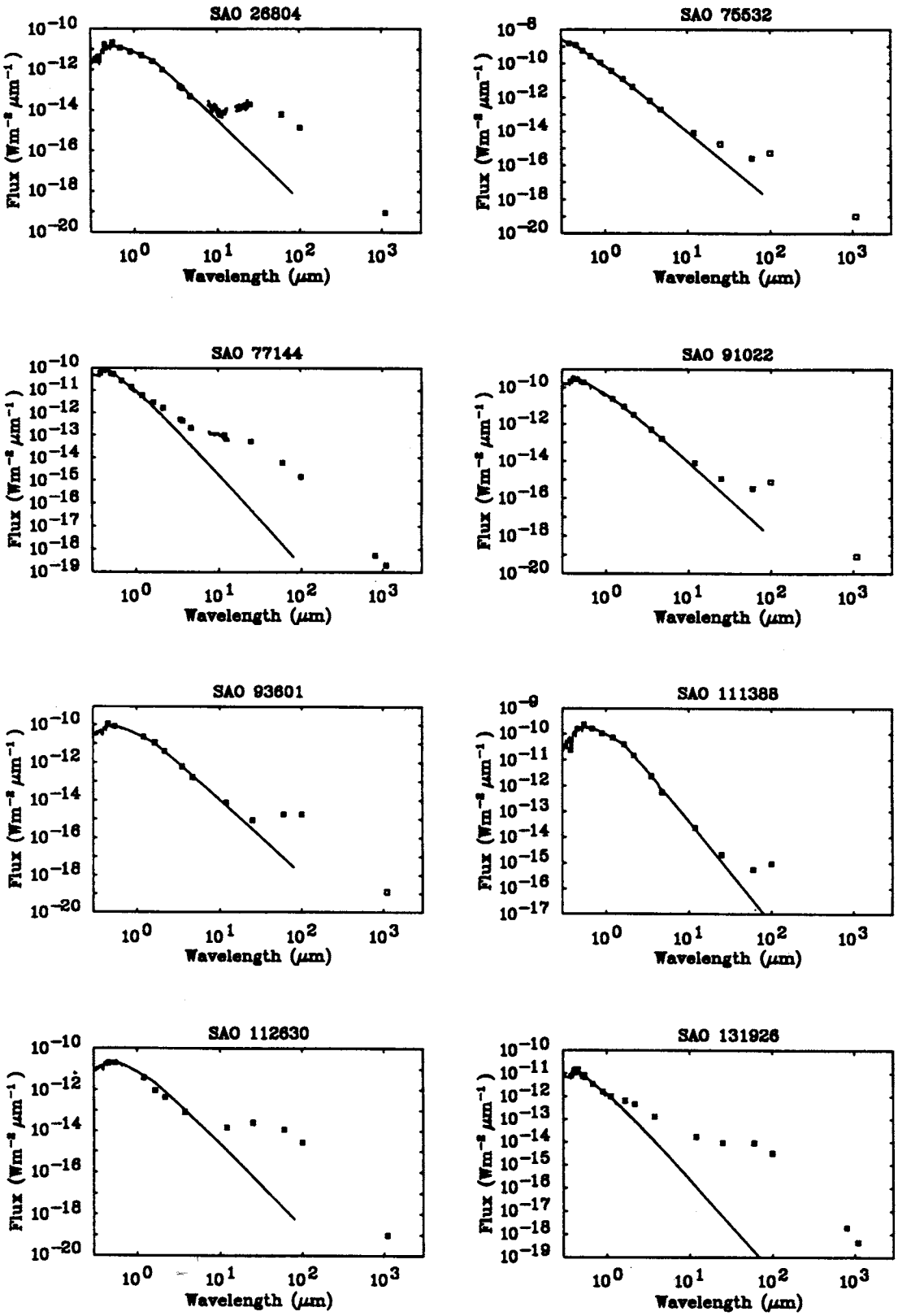

Figure 2. Spectral energy distributions of Vega-like stars. Large filled squares: dereddened photometry; small filled squares: CGS3 data; open squares: upper limits.

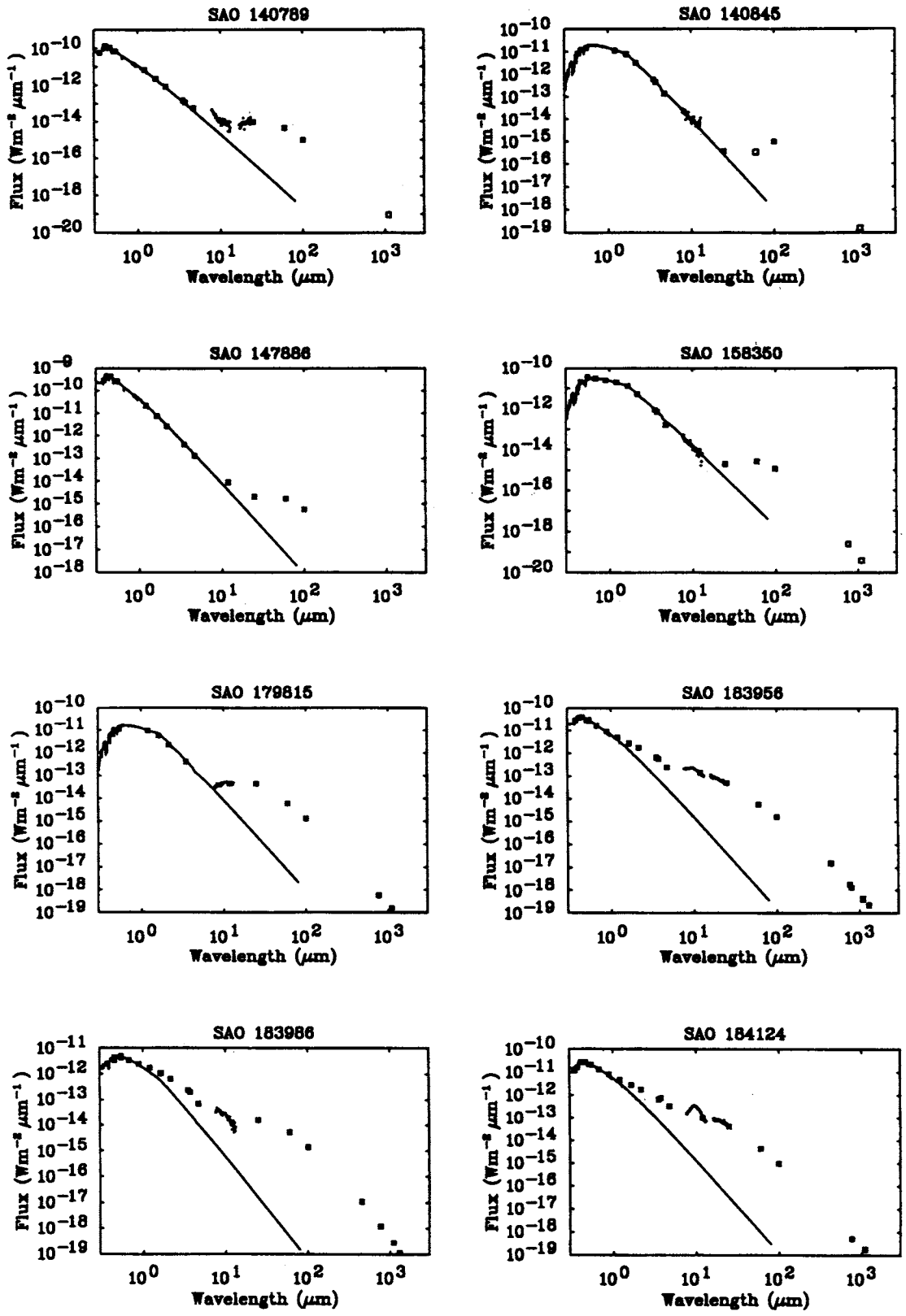

Figure 2 – *continued*

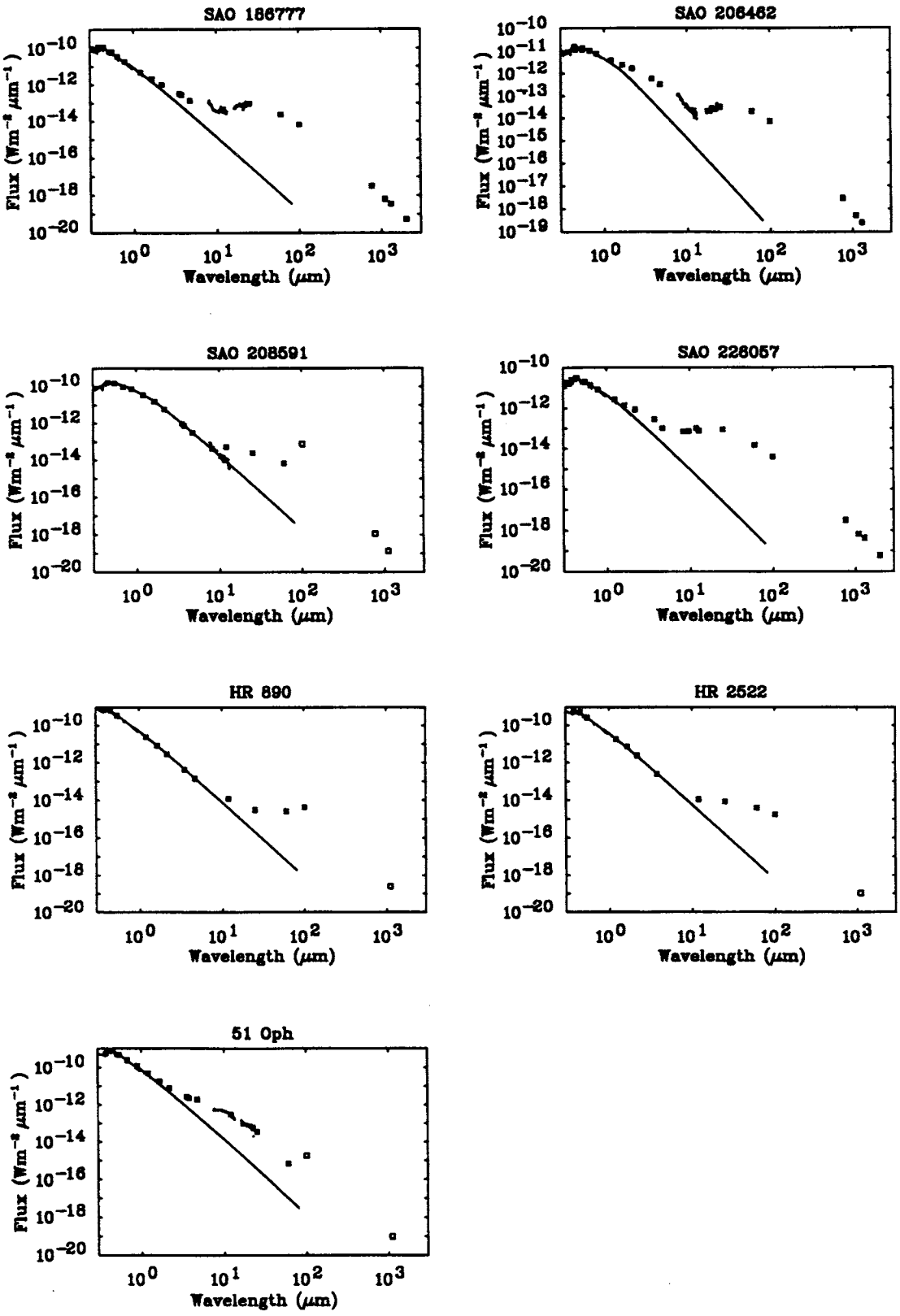

Figure 2 – *continued*

Table 11. Magnitude and colour temperatures of the near-IR excesses.

HD	SAO	Excess in magnitudes					T_{BB}
		J	*H*	*K*	*L*	*M*	(K)
34282	131926	0.2	1.1	1.9	2.8	–	1700
35187	77144	0	0.4	1.0	1.7	2.0	1800
135344	206462	0.3	0.8	1.4	2.5	2.9	1500
139614	226057	0	0.4	0.9	1.9	1.7	1500
142666	183956	0.2	0.6	1.2	2.2	2.2	1800
143006	183986	0.6	0.8	1.3	2.2	2.2	1500
144432	184124	0.2	0.6	1.2	2.0	2.6	1500
158643	185470	0	0.3	0.5	1.4	2.2	2000
169142	186777	0	0.4	0.8	1.5	1.7	1500

the values predicted by the model atmospheres, and then converting the ratios to magnitudes in the usual way. Subtracting the model atmosphere fluxes from the observed fluxes gave the energy distributions of the excess emission.

To gain some idea of the temperature of the material responsible for the near-IR excess (assuming it is thermal in origin), blackbodies were fitted to these excess spectra. The temperatures that gave the best fits are recorded in Table 11. In most cases it was not possible to fit all of the near-IR points with a single blackbody. In some cases, the observed excess energy distribution was broader than the Planck curve, suggesting that material at a range of temperatures contributed to the emission; in other cases, the observed distribution was narrower than a blackbody, suggesting that the emissivity of the material could be falling off with wavelength in the near-IR region.

Further insight into the near-IR properties of the Vega-like stars can be gained by plotting a colour–colour diagram. A $(J-H)$ versus $(H-K)$ diagram for the present sample is shown in Fig. 3. It shows two distinct groups of objects. The stars with no near-IR excess tend to lie near the locus expected for main-sequence stars, starting near the $(J-H)=(H-K)=0$ point and extending to $(H-K)\approx 0.2$, $(J-H)\approx 0.9$. The cooler stars have the redder colours, i.e. higher values of $(J-H)$.

The stars that do have a near-IR excess lie further to the right of the diagram, on a locus which coincides with that of the Herbig Ae/Be stars. We have plotted on the same diagram the colours of Herbig Ae/Be stars from Finkenzeller & Mundt (1984), classical T Tauri stars (CTTS) from Rydgren et al. (1984) and weak-lined T Tauri stars (WTTS) from Walter et al. (1988). The $(J-H)$ colours of the Vega-like stars with a near-IR excess lie within the range spanned by the cooler of the stars without a near-IR excess. This is consistent with the fact that near-IR excesses contribute a negligible amount to the flux at *J*, and make only a small contribution at *H*. The net effect of this is to produce colours that mimic those of a somewhat cooler stellar photosphere.

The observed excesses make a more significant difference to the flux at *K* (see Table 11), giving rise to $(H-K)$ colours that do not resemble the photospheric colours of normal main-sequence stars, therefore causing the points in the colour–colour diagram to be significantly displaced with respect to those of the stars that show only photospheric emission. Similar diagrams have been produced before for pre-main-sequence stars (see e.g. Hillenbrand et al. 1992; Lada & Adams 1992).

An $(H-K)$ versus $(K-L)$ diagram for the same samples of stars is plotted in Fig. 4. Taken together, these two diagrams reveal that at least some of the Vega-like stars are likely to be related to the Herbig Ae/Be stars, perhaps descended from them. Others give the impression that they may be related to the WTTS. The Vega-like stars may thus include stars with masses that are quite low all the way through to the intermediate-mass range spanned by the Herbig Ae/Be stars. This would be in accord with the suggestion already made (Backman & Paresce 1993) that the Vega-like stars may generally be in an intermediate evolutionary stage between pre-main-sequence stars, such as T Tauri or Herbig Ae/Be stars, and the main sequence.

The near-IR observations made with IRCAM can give spatial, as well as photometric, information. To determine if anything could be gleaned about the spatial distribution of the material responsible for the near-IR excess, the full widths at half maximum of the IRCAM images of the two imaged stars with near-IR excesses, SAO 186777 and SAO 131926, were measured. It was found that the FWHM for both these targets and for the standard stars were similar. At 3.3 μm, SAO 186777 had a FWHM of 2.2 pixels in the north–south direction and 1.8 pixels in the east–west direction, compared with 2.2 and 1.7 pixels for Y4338. At *K* (2.2 μm), SAO 131926 measured 2.1 pixels in the N–S direction and 1.6 pixels E–W, compared with 2.0 and 1.8 pixels for HD 22686. There is therefore no evidence that the two target stars are extended in the near-IR compared with the standard stars.

Both stars show substantial excess emission at these wavelengths and the dominant source of emission is presumably hot circumstellar matter. The hot material must therefore be concentrated within a radius of approximately 0.6 arcsec of the exciting stars, which corresponds to 140 au and 340 au at the distances of SAO 186777 and SAO 131962 respectively. By contrast, the near-IR emission from reflection nebulae, attributed to thermally spiking grains by Sellgren, Werner & Dinerstein (1983), is extended over distances ~ 0.15 pc.

4.3 Mid-IR spectral features

The Vega-like stars in our sample that show significant excesses at 10 μm display spectral features which can be divided into two categories: either a broad emission feature centred on a wavelength of approximately 9.7 μm, or a set of narrower bands, dominated by one at 11.3 μm and one peaking shortward of 8 μm, of which we see only the long-wavelength wing.

It is harder to pick out features in the 20-μm spectra, partly because they tend to be noisier than their 10-μm counterparts due to poorer atmospheric transmission than in the 10-μm window. In the case of SAO 183956, SAO 184124 and SAO 185470, plotting the combined 10- and 20-μm spectra suppresses the contrast in the 20-μm region due to the flux levels in the 10-μm spectra being significantly higher than at 20 μm. For these three cases, the 20-μm spectra have also been plotted separately in order to emphasize any features (see Fig. 5). The log–log scaling used on the spectral energy distribution plots (Fig. 2) also helps emphasize weak 20-μm features. A feature does appear to be present in some cases, e.g. SAO 184124, namely a broad emission feature peaking at around 18–19 μm.

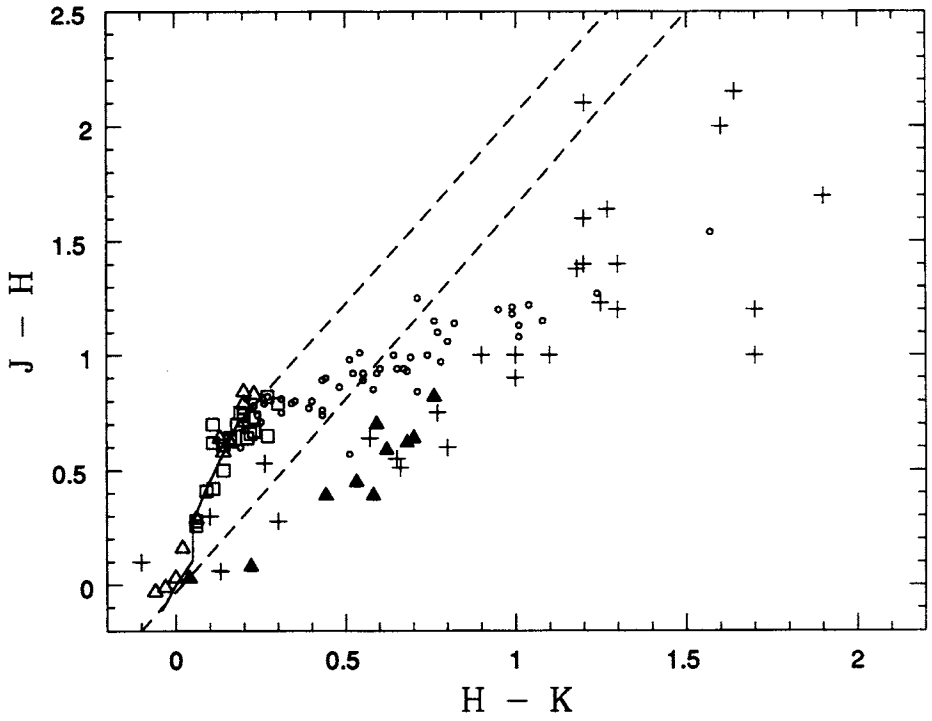

Figure 3. Near-IR $(J-H)$ versus $(H-K)$ colour–colour diagram for Vega-like and pre-main-sequence stars. Open triangles: Vega-like stars without discernible near-IR excess; filled triangles: Vega-like stars with near-IR excess; crosses: Herbig Ae/Be stars; open squares: WTTS; open circles: CTTS. Dashed lines are reddening tracks.

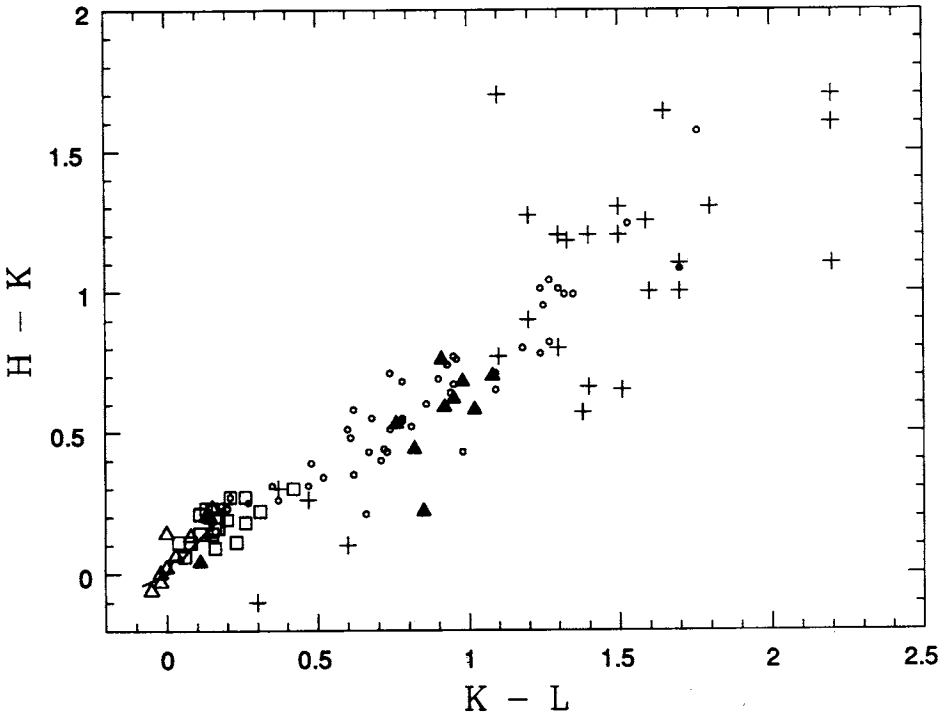

Figure 4. $(H-K)$ versus $(K-L)$ diagram for Vega-like and pre-main-sequence stars. Symbols as for Fig. 3.

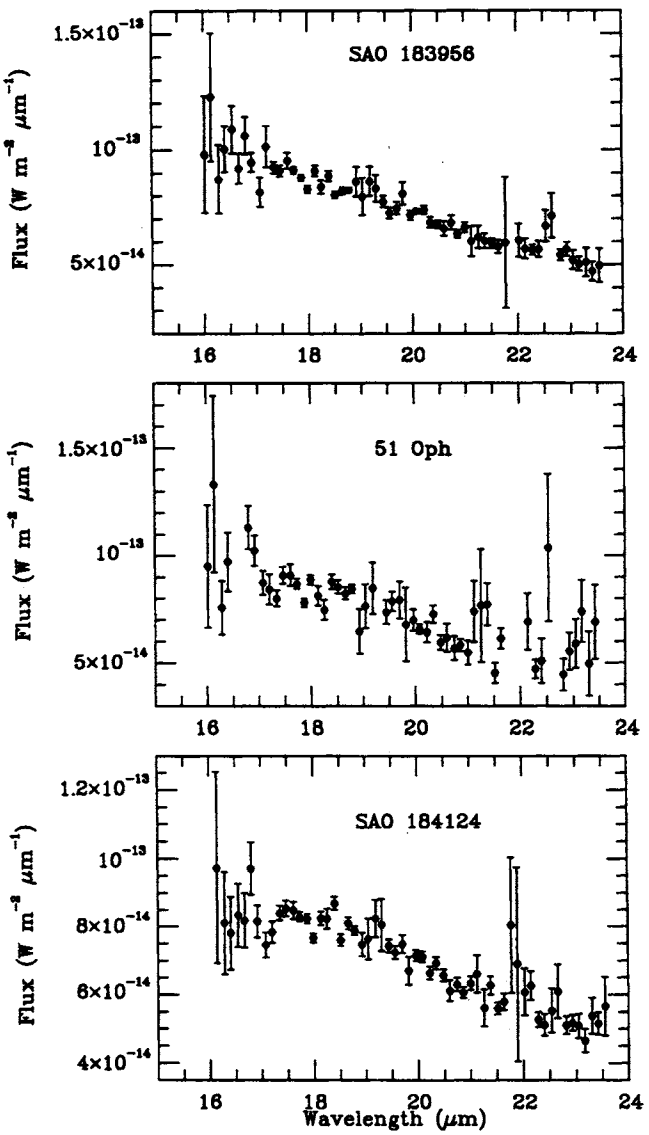

Figure 5. 20-μm spectra enlarged for clarity.

The feature peaking at approximately 9–10 μm in the mid-IR spectra of some sources has long been recognized as due to circumstellar silicate grains (see e.g. Woolf & Ney 1969; Gilman 1969). Silicate emission is clearly present in the 10-μm spectra of five of our sources (SAO 179815, 183956, 184124, 77144 and 185470) and it appears to be present in the spectra of two others (SAO 26804 and SAO 183986) as a rather weak, narrow feature.

The strong terrestrial ozone emission feature around 9.5 μm can lead to spurious features in ground-based mid-IR spectra, because it can be strongly time variable and thus difficult to cancel. However, this feature typically has a full width of only about 0.8 μm, and the features observed in SAO 26804 and SAO 183986 are much broader than this, and more consistent with astronomical silicate features. The broad emission bump seen at 18 μm in the spectra of SAO 179815, 184124, 186777, 206462, and 185470 is also attributable to silicate materials.

Many sources in the *IRAS* Low-Resolution Spectrometer (LRS) atlas (Neugebauer et al. 1986) show silicate emission features. A measure of the strength of the silicate band is defined in the LRS atlas as:

$$B_{\rm sil} = 10 \times \ln f_\lambda(9.8\ \mu{\rm m}) - [5.89 \ln f_\lambda(7.9\ \mu{\rm m}) + 4.11 \ln f_\lambda(13.3\ \mu{\rm m})] \quad (1)$$

where f_λ is the spectral flux density. $B_{\rm sil}$ is thus a measure of the ratio of the power emitted in the silicate band to that emitted in the underlying continuum. For the five stars with obvious silicate emission, the derived values of $B_{\rm sil}$ are given in Table 12.

Table 12. CGS3 spectra: derived quantities.

HD	SAO	$B_{\rm sil}$	$\frac{F_{10,\rm exc}}{F_{10,\rm phot}}$	K_{12}
35187	77144	2.9	66	1.11
98800	179815	6.4	5.0	0.93
123160	158350	–	0	1.41
135344	206462	–	17	1.50
141569	140789	–	3.6	1.32
142666	183956	4.9	273	1.23
142764	140845	–	0	0.96
143006	183986	–	3	1.38
144432	184124	10.7	186	1.52
155826	208591	–	0	1.40
158643	185470	2.5	28	1.11
169142	186777	–	20	1.30
233517	26804	–	2.1	1.38

The values we obtain cover a wide range of silicate strengths, comparable to those found for a sample of O-rich cool stars by Skinner & Whitmore (1988). The value of $B_{\rm sil}$ = 10.7 for SAO 184124 is one of the highest known, as evidenced by the fact that the definition of $B_{\rm sil}$ was chosen so that the majority of stars with silicate emission would give values that lie between 1 and 9 (the maximum value quoted in the LRS atlas).

The UIR bands are generally ascribed to UV-pumped IR fluorescence by aromatic structures, e.g. large aromatic molecules, such as PAHs (Léger & Puget 1984; Allamandola, Tielens & Barker 1985), or hydrogenated amorphous carbon (HAC) particles (Duley & Williams 1981). The strongest of these bands in the mid-infrared lie at approximately 7.7, 8.7, 11.3 and 12.7 μm.

11.3-μm UIR-band emission is definitely present in the 10-μm spectrum of SAO 186777 and is probably present in the spectra of four other Vega-like stars: SAO 26804 (see Skinner et al. 1995 for a detailed discussion of this source), SAO 140789, 183986, and 206462. A strong 7.7-μm feature is clearly present in the spectra of all five of these sources. Although the peak of the 7.7-μm feature lies at a shorter wavelength than the short-wavelength extreme of the observed spectra, the fact that the 7.8–10 μm slopes of the spectra of these five sources are significantly steeper than a Rayleigh–Jeans energy distribution implies that a feature is truly present, rather than the emission being due to some combination of blackbodies. The 8.7-μm band is present in the spectrum of SAO 186777 and possibly that of SAO 206462. There is no correlation between the presence of UIR bands and spectral type: the five stars with UIR bands are distributed evenly across the range B9–K2. Since the UIR bands are thought to be excited by UV photons, it might have been expected that the incidence of UIR-band

emission would be higher for the hotter stars. This would seem to imply that the later-type stars have excess UV flux above that expected from a normal photosphere. Radiative-transfer modelling of the present sample of Vega-like systems (Sylvester et al., in preparation) has shown that the flux in the 7–9 μm portion of the spectra of SAO 77144 and SAO 183956 was in excess of that predicted to arise from the short-wavelength wing of a silicate feature. The residual emission was very suggestive of the presence of a UIR component in the emission from these two stars.

The good agreement found in almost all cases between the CGS3 fluxes and the colour-corrected *IRAS* 12-μm fluxes, as well as confirming the accuracy of the CGS3 flux calibration, provides some spatial information, since, if a source were significantly extended at 10 μm with respect to the CGS3 beam, CGS3 would have detected less flux than *IRAS*, which has a much larger beam. Since for the vast majority of our sources the CGS3 and *IRAS* 12-μm fluxes are nearly identical, we can conclude that the objects are not significantly extended compared with the 5.5-arcsec diameter CGS3 beam. In all three cases where we see a large discrepancy, the *IRAS* flux is higher than the CGS3 flux.

For one of the three sources, SAO 208591, the large *IRAS* fluxes are probably due to source confusion, as discussed in Section 3.3. The other two sources, SAO 77144 and SAO 186777, might be extended with respect to the CGS3 beam, but mid-IR imaging is required to confirm this.

Table 12 presents values of the relative excess flux at 10.0 μm ($F_{10,\mathrm{exc}}/F_{10,\mathrm{phot}}$) and of the 12-$\mu$m colour correction factor (K_{12}), derived from our CGS3 spectra.

4.3.1 *Notes on individual sources*

SAO 179815: The 10-μm spectrum of SAO 179815 (Fig. 1a) shows a fairly broad silicate feature superposed on a continuum rising towards longer wavelengths. The feature appears to peak at a wavelength slightly longwards of 10 μm, whereas the 'typical' silicate feature peaks at around 9.7 μm. In this respect, it is similar to the h and χ Per M-type supergiants having *IRAS* 12-μm fluxes less than 21 Jy that were observed by Sylvester, Barlow & Skinner (1994a).

The points at the short-wavelength end of the 10-μm spectrum lie only slightly higher than the expected photospheric spectrum – it would be interesting to extend the spectral coverage to include the 5–8 μm region, where the changeover between the photospheric and dust-dominated emission régimes is expected to take place. While this waveband is unobservable from the ground, these observations could be made with the *Infrared Space Observatory* (*ISO*), and are included in the *ISO* Short-Wavelength Spectrometer (SWS) Consortium programme. It is not clear whether or not the apparent sharp upturn in the spectrum at 13 μm is real; *ISO* observations will also cover the 14–16 μm region and should resolve this question.

The 20-μm spectrum shows a weak feature peaking at about 19 μm (most easily discerned in the overall energy distribution plot in Fig. 2), presumably the '18-μm' silicate feature, but the spectrum is rather noisy. The overall flux level in the 20-μm spectrum is higher than in the 10-μm spectrum, and the levels of the spectra are in accord with the *IRAS* 12- and 25-μm fluxes.

SAO 183956: The spectrum of SAO 183956 (Fig. 1b) is qualitatively different from that of SAO 179815. The 10-μm region shows a falling continuum, upon which is superimposed a silicate feature peaking at about 9.5 μm. The peak itself is somewhat obscured by the noise due to the telluric ozone band, but its position can be interpolated from the uncontaminated points. Longwards of the emission peak, the spectrum starts to level off, until approximately 11.3 μm, where there is a point of inflection, after which the spectrum starts to fall more rapidly again. The 10-μm excess is very large, with a ratio of excess flux to expected photospheric flux at 10.0 μm of 273 – the largest value measured for any of the sources. Note that there is a discrepancy (of about 20 per cent) between the flux level and that of the *IRAS* 12-μm point, i.e. roughly three times the uncertainty in the PSC value.

SAO 184124: This star shows a remarkably strong 10-μm silicate feature (Fig. 1c) peaking at about 9.5 μm. Again the peak is rather noisy due to ozone contamination. As noted earlier, the B_{sil} value, 10.7, is the highest for any source in the sample. Also, as for SAO 183956, there is a secondary bump at about 11 μm on the wing of the silicate feature; it is somewhat smoother than that of SAO 183956. The colour-corrected *IRAS* flux is in excellent agreement with the CGS3 spectrum at 12.0 μm. The 18-μm silicate feature is visible as curvature in the 20-μm spectrum (see Fig. 5 and the overall energy distribution in Fig. 2).

SAO 185470 (51 Oph): The 10-μm spectrum of SAO 185470 is peculiar, and is composed of two almost linear portions at 8–8.7 and 10–13 μm, with a bump at 9.0–9.5 μm (Fig. 1d). The bump is due to poor ozone cancellation – on reducing this spectrum it was found that none of the standard star observations was fully able to cancel the ozone feature. The slope of the short-wavelength part of the spectrum was also slightly dependent on the choice of standard star. Subtracting a continuum fit to the spectrum at 8 and 13 μm leaves a broad emission feature peaking at around 10 μm. The 20-μm spectrum clearly shows the 18-μm silicate feature superposed on a downward-sloping continuum (Fig. 5).

The agreement between the colour-corrected *IRAS* 12-μm flux and the CGS3 spectrum is excellent, implying that the flux calibration of the CGS3 spectrum is good. Fajardo-Acosta, Telesco & Knacke (1993) obtained narrow-band ($\lambda/\delta\lambda \sim 10$) photometry of SAO 185470 from 7.8 to 21.9 μm. Their data are plotted in Fig. 1(d) as open circles. Their spectrum has approximately the same shape as ours, but their points tend to be lower than the CGS3 data. Since the absolute flux calibration of the CGS3 spectrum is in agreement with that of *IRAS*, it would appear that there is a slight error in the calibration of the Fajardo-Acosta et al. data. The 7.8–8.7 μm slope in their photometry is slightly steeper than in the CGS3 spectrum, although both spectra have large errors shortward of 8 μm – the 7.8-μm point is at the edge of the 10-μm atmospheric window, so that flux calibration here is difficult.

SAO 186777: This was the first Vega-like star to have UIR-band emission detected in its 10-μm spectrum (Sylvester et al. 1994b). The CGS3 spectrum (reproduced in Fig 1e) shows the long-wavelength wing of a strong 7.7-μm band. There seems to be a narrow 8.7-μm UIR feature superposed on the wing of the 7.7-μm band, but, since it is only defined by a couple of data points, it might be an artefact. Higher-resolution mid-IR spectroscopy could help to determine the reality (or otherwise) of the feature. SAO 186777 is in the *ISO* SWS Consortium Guaranteed Time programme. From 9 to

Table 13. Expected spectral indices for different conditions.

		R–J	non R–J
Optically Thin	Turned-over	$2+\beta$	$< 2+\beta$
	Grey	2	< 2
Optically Thick		2	< 2

10.5 μm, there is a smooth continuum with a slight downward slope to longer wavelengths.

There is a strong, well-defined emission peak extending from 11.0 to 11.6 μm and peaking at 11.3 μm, clearly the 11.3-μm UIR feature. The spectrum starts to rise again at 12.3 μm, and seems to be levelling off at 12.6 μm, before breaking up and becoming noisy. This is probably the 12.7-μm UIR band. The *IRAS* 12-μm point lies significantly above the CGS3 spectrum at 12.0 μm. Since the colour-correction technique takes into account the detailed shape of the spectrum, this cannot be ascribed to the fact that the spectrum is dominated by emission bands. The 20-μm spectrum is noisy, but shows the 18-μm silicate feature.

SAO 206462: The spectrum of this source shows the 7.7-μm UIR band, with a subsidiary bump which is probably the 8.7-μm band (Fig. 1f). The 9.5–10.0 μm region is noisy, due to ozone contamination. From 10 to 13 μm, the spectrum shows a gently falling continuum, with a weak 11.3-μm bump. The *IRAS* 12-μm point lies slightly above the CGS3 12.0-μm point. The 20-μm spectrum shows a general increase of flux with wavelength, but exhibits no obvious spectral features. The shape of the 10-μm spectrum is in good agreement with that of the spectrum obtained by Coulson & Walther (1995).

4.4 The mm-wave flux distributions

The long-wavelength Rayleigh–Jeans (R–J) portion of a blackbody spectrum behaves as $F_\nu \propto \lambda^{-2}$, i.e. $\alpha = 2$. The absorption (or, equivalently, emission) efficiency of a grain is approximately constant ('grey' emission) at wavelengths shortward of a turnover wavelength, $\lambda_T \approx 2\pi a$, where a is the grain radius (e.g. Bohren & Huffman 1983). Longwards of λ_T, the grain emissivity ε_λ (or absorption) falls as $\lambda^{-\beta}$, where β is typically in the range 1–2 (see e.g. Pollack et al. 1994 for some computed values of β). In real materials, the turnover does not occur abruptly, but occurs over some wavelength interval. The observed spectral index for a single grain emitting in the R–J domain will therefore be $\alpha = 2$ for $\lambda < \lambda_T$ and $\alpha = 2+\beta$ for $\lambda > \lambda_T$.

The submm spectral index of a dust disc depends on three factors: the optical depth of the disc, the temperature distribution, and the grain emissivity. Simplistically, we can describe these in terms of three pairs of possibilities – whether or not the disc is optically thick in the submm region, whether or not the emission from the dominant grains (whichever they happen to be) is in the R–J régime in the submm, and whether or not the emission from these grains has 'turned over'. The expected spectral indices for the various combinations of these possibilities are presented in Table 13.

Spectral indices have been determined for the observed Vega-like stars, and are presented in Table 14. Uncertainties are calculated from the uncertainties on the flux measurements, and on the quoted uncertainties in the *IRAS* PSC fluxes where appropriate. Where only upper limits to the mm-wave flux were obtained, lower limits to the value of α are quoted.

These observed values can be compared with those derived for three of the prototype Vega-like stars: Vega, β Pic and Fomalhaut. Some care needed to be exercised in selecting the observed fluxes to be used for the prototypes since, for example, the faint mm-wave source Fomalhaut is slightly extended‡ compared with the 11-arcsec beam of the 30-m IRAM telescope (Chini et al. 1991), but not compared with the 24-arcsec SEST beam (Chini et al. 1994; Stern et al. 1994b). The 0.87-mm IRAM observations of Vega-like sources by Chini et al. (1990) and the 0.8-mm JCMT observations by Zuckerman & Becklin (1993) are admitted by both sets of authors to be inconsistent.

Weintraub & Stern (1994) raised the possibility that the two sets of measurements need not be inconsistent if the emitting regions are extended with respect to the largest beamsizes used. However, the observations of Chini et al. (1994) showed this is not the case for Fomalhaut, so the inconsistencies remain for this star and, assuming that calibration problems are responsible, for the other stars as well. We use the Zuckerman & Becklin total flux measurements at 0.8 mm, obtained by summing the contributions from a number of beams positioned on-source and offset by about a beamwidth, and the Chini et al. (1991) SEST measurements, which have a larger beam than the earlier IRAM observations. The spectral indices derived in this fashion are presented in Table 15.

There is clearly a difference between the spectral indices of the prototypes and those of our sources. The prototypes all show $\alpha > 2$ in the 100 μm–0.8 mm region which, from Table 13, indicates that the grain emissivity for these sources has already started to turn over, i.e. that the turnover wavelength occurs somewhere within the 100 μm–0.8 mm region. The 60–100 μm spectral indices of α Lyr, β Pic and α PsA are 0.4, 1.1 and 0.4 respectively, suggesting that turnover has not occurred shortwards of 100 μm.

The maximum grain size in these systems is therefore of the order of several tens to one hundred microns. Backman & Paresce (1993) estimated typical grain sizes of 80, 27 and 1 μm for Vega, Fomalhaut and β Pic respectively, while Artymowicz et al. (1989) derived an upper limit of 15 μm for the maximum grain size in the β Pic disc. However, Zuckerman & Becklin (1993) found that grains of radius larger than 100 μm must be present in the discs of Vega, Fomalhaut and β Pic based on the 800-μm opacities calculated by Pollack et al. (1994). The 0.8–1.3 mm spectral indices, although having rather high uncertainties, show values consistent with turned-over emission in the R–J domain. In the cases of Vega and Fomalhaut, the values are close to 4, implying R–J emission and grain emissivity varying as λ^{-2}, consistent with the value expected for crystalline materials.

Our programme sources, on the other hand, have much lower spectral indices (Table 14) – typically less than 2. Only one system, SAO 206462, appears to show turned-over emission, while three others, SAO 112630, 131926 and SAO 226057, have spectral indices larger than 2, but values of 2 would

‡ Note that a recent report of a bright, extended region of 1.3-mm emission around Fomalhaut (Stern, Festou & Weintraub 1994a) has been retracted (Stern, Festou & Weintraub 1994b; Chini et al. 1994).

Table 14. Observed submm spectral indices for the programme sources.

HD	SAO	$\alpha_{0.1-0.45}$	$\alpha_{0.1-0.8}$	$\alpha_{0.1-1.1}$	$\alpha_{0.45-0.8}$	$\alpha_{0.45-1.1}$	$\alpha_{0.8-1.1}$	$\alpha_{0.8-1.3}$
18537	23763	–	–	> 2.5	–	–	–	–
23680	93601	–	–	> 2.0	–	–	–	–
34282	131926	1.4±0.2	1.61±0.06	1.70±0.06	2.0±0.4	2.2±0.2	2.5±0.4	–
34700	112630	–	–	2.2± 0.1	–	–	–	–
35187	77144	–	1.8±0.1	1.72±0.07	–	–	1.1±0.7	–
49662	151962	–	–	> 2.0	–	–	–	–
98800	179815	–	1.82±0.07	1.78±0.06	–	–	1.5±0.4	4.8±1.1
123160	158350	–	> 2.3	> 2.3	–	–	–	–
135344	206462	–	1.83±0.05	2.01±0.05	–	–	2.8±0.2	2.9±0.3
139614	226057	–	1.55±0.07	1.65±0.06	–	–	2.2±0.2	1.89±0.2
141569	140789	–	–	> 1.9	–	–	–	–
142666	183956	1.07±0.05	1.35±0.04	1.05±0.05	2.2±0.2	2.1±0.1	2.0±0.2	2.1±0.2
142764	140845	–	–	> 1.8	–	–	–	–
143006	183986	0.96±0.08	1.49±0.07	1.56±0.04	3.0±0.2	2.6±0.2	1.9±0.4	2.7±0.3
144432	184124	–	1.7±0.2	1.59±0.08	–	–	1.0±0.5	–
169142	186777	–	1.84±0.06	1.84±0.05	–	–	1.78±0.08	2.1±0.2
233517	26804	–	–	> 2.0	–	–	–	–

still be consistent within the errors. Three stars, SAO 77144, SAO 179815 and SAO 184124, have 0.8–1.1 mm spectral indices which are very slightly lower than the 100 μm–0.8 mm spectral indices, although they are consistent within the 1σ errors. We consider this more likely to be an artefact, due to imperfect calibration of one of the submm flux densities, than a real feature, since a real feature would imply a sudden increase in mass at low temperatures compared with the amount of mass at slightly higher temperature.

From Table 13 we see that a spectral index of less than 2 implies that the material is not emitting in the R–J régime at the observed wavelengths, regardless of whether or not the grain emissivity has turned over. There are thus three possible explanations for the observed spectral indices.

(i) The grain emissivity has turned over, but the grain emission is far from the R–J domain, and so the Planck function is falling very slowly (or even rising).

(ii) The grain emissivity has not turned over – i.e. greybody emission.

(iii) The disc is optically thick at mm wavelengths, and so the emission is like that of a collection of blackbodies.

All three of these situations require that the grain emission is not in the R–J domain.

If the grain emission has turned over (i.e. $\lambda > \lambda_T$), the slope of the equivalent blackbody spectrum must be very shallow and far from the R–J domain, implying very low temperatures. For example, an observed spectral index between 0.8 and 1.1 mm of slightly less than 2 with grains having an emissivity $\varepsilon_\lambda \propto \lambda^{-1.5}$ would require the modified Planck function to have a mm-wave spectral index of just under 0.5, implying that the emission is dominated by material at a temperature of 7 K. Since cool blackbodies emit less energy at all wavelengths than do hotter ones, there would need to be much more mass at low temperatures (i.e. in the cool outer parts of the disc) than at higher temperatures (further in towards the star). This is contrary to the normal expectations of disc structure, according to which the outer parts of the disc are less densely populated by the grains. Radiative-transfer modelling of the entire spectral energy distribution (Sylvester et al., in preparation) is needed in order to determine whether emission from grains with $2\pi a \ll \lambda$ can be responsible for the observed submm spectral indices.

Table 15. Submm spectral indices for prototype Vega-like stars.

Star	$\alpha_{0.1-0.8}$	$\alpha_{0.8-1.3}$
α Lyr	2.7±0.3	3.9±1.2
β Pic	2.4±0.1	3.2±0.6
α PsA	2.8±0.1	4.1±0.5

Optically thick emission behaves like blackbody radiation even for wavelengths longer than the turnover wavelength (see e.g. Adams, Lada & Shu 1988), and therefore gives rise to a spectral index indistinguishable from that due to emission by large greybody grains. One could calculate the optical depth of the emission from a model of the dust disc, and then determine whether optically thick conditions apply.

It is worth noting that the mm-wave emission from a sample of Herbig Ae/Be stars (Mannings 1994), which are the possible precursors of some Vega-like stars, is optically thin (as judged from the mm/submm spectral indices) in most cases. The later stages of the standard evolutionary scenario have the discs clearing by grains either falling on to the star or being expelled from the system, and by grain coagulation (e.g. Shu, Adams & Lizano 1987). Thus, one would expect a priori that, following formation of a circumstellar disc and, later, the termination of infall at the outer boundary of the disc from the circumstellar envelope, the disc optical depth would not increase with time, but the maximum grain size would. Larger grains could therefore appear more plausible than optically thick emission as the cause of the shallower spectral indices observed for the Vega-like sources, compared with the Herbig Ae/Be stars.

In summary, it can be said that, unlike the prototype Vega-like sources, the objects discussed here are not emitting in the R–J domain, and detailed modelling (Paper 2) is required to determine whether turnover has been achieved, and whether the emission is optically thick.

5 OVERALL SPECTRAL ENERGY DISTRIBUTIONS AND THE FRACTIONAL DUST DISC LUMINOSITIES

Combining all the new observations with the *IRAS* data enables the optical–mm spectral energy distribution (SED) for each source to be defined. The SEDs for the present sample of Vega-like stars are presented in Fig. 2. The observations have been dereddened using the observed $(B-V)$ colours and the tabulated intrinsic colours as a function of spectral type of Schmidt-Kaler (1982), assuming the Galactic reddening law of Howarth (1983), with $A_V = 3.1E(B-V)$.

Fitting a model atmosphere to the dereddened optical photometry makes it possible to calculate the fractional luminosity of the dust, $L_{IR}/L_\star$, the ratio of the total energy radiated (in the IR–submm) by the dust, L_{IR}, to the stellar luminosity, $L_\star$. $L_{IR}/L_\star$ gives a useful indication of the optical depth of the disc material. For optically thin emission, $L_{IR}/L_\star$ is in fact equal to the fraction of the sky as seen from the star that is occupied by dust. For a flat optically thick disc, the maximum value of $L_{IR}/L_\star$ is 1/4, while for a 'flared' disc, i.e. one in which the azimuthal thickness increases with distance from the star, $L_{IR}/L_\star$ can reach values of approximately 1/2 (Kenyon & Hartmann 1987). The prototype Vega-like stars have $L_{IR}/L_\star \sim 10^{-5}$–$10^{-3}$ (e.g. for β Pic $L_{IR}/L_\star = 2.6 \times 10^{-3}$). Such low values indicate that the dust discs have very low optical depths at all wavelengths.

Table 16 presents the values of $L_{IR}/L_\star$ derived for the present sample of Vega-like stars, which were calculated as follows. First, a smooth curve representing the observed (but dereddened) energy distribution was constructed by fitting a spline to the photometric points from the optical to the submm region. The photospheric contribution is represented by an appropriate Kurucz (1991) model atmosphere normalized to the dereddened optical photometry. The two curves were then plotted and inspected to ascertain at what wavelength the observed energy distribution diverges from that expected from the star, i.e. the shortest wavelength with excess emission. The total observed and expected (photospheric) fluxes in the excess region were then determined by integrating under each curve longwards from this point with the photospheric continuum being subtracted from the observed flux to give the excess IR luminosity, L_{IR}. Integrating under the model atmosphere over its complete wavelength range then gave the stellar luminosity, $L_\star$, finally allowing the ratio $L_{IR}/L_\star$ to be derived.

The observed values of $L_{IR}/L_\star$ show a strong anti-correlation with the shortest wavelength at which an excess is discernible (see final column of Table 16). For example, the stars with no excess at 12 μm have fractional luminosities of around 10^{-5} – 10^{-3}, while those with a 12-μm excess but no near-IR excess have values from about 10^{-3} to nearly 10^{-1}. The stars with near-IR excesses have the largest values of $L_{IR}/L_\star$, approximately in the range 0.1–0.6. This is not surprising, given that stars emit more of their luminosity at visible and near-IR wavelengths rather than in the far-IR, so, for a short-wavelength excess to be discernible above the photospheric flux, it must necessarily be very luminous.

While several of the stars in Table 16 have values of $L_{IR}/L_\star$ comparable to those of the 'prototype' Vega-like stars (e.g. SAO 93601, SAO 140789 and SAO 158350), others show values substantially larger, some of which exceed the 'flat disc' maximum of 0.25 (SAO 131926, SAO 226057, SAO 206462, SAO 183956, SAO 183986, and SAO 184124). The largest value obtained is 0.64 for SAO 206462 (in good agreement with the results of Coulson & Walther 1995), implying that almost two-thirds of the stellar radiation is reprocessed before escaping from the stellar system. Given a disc-like geometry for the dust, such a large IR excess is not possible by passive thermal reprocessing by grains alone. This implies either an additional source of IR luminosity, or an alternative geometry for the dust.

Table 16. Fractional excess IR luminosities ($L_{IR}/L_\star$) of Vega-like stars and shortest wavelength of excess emission.

HD	SAO	$L_{IR}/L_\star$	$\lambda_{sh}(\mu m)$
9672	147886	8.7×10^{-4}	12
16908	75532	1.8×10^{-5}	60
18537	23763	8.7×10^{-4}	12
23362	111388	7.9×10^{-4}	25?
23680	93601	3.0×10^{-3}	25
34282	131926	0.39	1.2
34700	112630	0.15	12
35187	77144	0.14	1.7
49662	151962	1.1×10^{-3}	12
98800	179815	0.084	12
123160	158350	4.4×10^{-3}	25
135344	206462	0.64	1.7?
139614	226057	0.39	1.7
141569	140789	8.4×10^{-3}	3.5
142666	183956	0.34	1.2
142764	140845	1.7×10^{-3}	100
143006	183986	0.56	1.2
144432	184124	0.48	1.7
158643	185470	0.028	2.2
169142	186777	0.088	1.65
218396	91022	1.8×10^{-4}	25
233517	26804	0.077	12

Cohen, Emerson & Beichman (1989) calculated $L_{bol}/L_\star$ ($\equiv L_{IR}/L_\star + 1$) for a large sample of T Tauri stars, using a method similar to that used here for the Vega-like stars. Table 17 shows some of their results, converted into $L_{IR}/L_\star$ for comparison with the values in Table 16. Cohen et al. found that values of $L_{bol}/L_\star$ for 'typical' T Tauri stars ranged up to approximately 2.4, with one-third of the sample having $L_{bol}/L_\star \approx 2$ (i.e. $L_{IR}/L_\star$ values of 1.4 and 1 respectively). T Tauri stars with [O I] emission, indicative of mass outflow, had larger values of $L_{bol}/L_\star$, ranging up to roughly 4.

Table 17 also presents values of $L_{IR}/L_\star$ for a number of Herbig Ae/Be stars. The values were calculated in the same way as for the Vega-like stars, using data from Hillenbrand et al. (1992). All four Ae/Be stars in Table 17 were from the Hillenbrand et al. Group I; such objects are thought to be the intermediate-mass counterparts of T Tauri stars, and to have substantial accretion discs. The values for three of the four Ae/Be stars lie in the same range as those of the Vega-excess stars, while the fourth, BF Ori, has a much larger fractional excess luminosity than any of the Vega-like stars in Table 16. We note that the value obtained for BD+40 4124 is sufficiently low that no accretion luminosity need be postulated for this source.

It appears that the fractional excess luminosities of several

Table 17. Fractional excess IR luminosities (L_{IR}/L_*) of T Tauri stars (upper part; values derived from Cohen et al. 1989) and of Herbig Ae/Be stars (lower part; calculated from data in Hillenbrand et al. 1992).

Star	L_{IR}/L_*
T Tau N	1.67
BP Tau	0.19
DE Tau	1.38
GK Tau	1.16
HK Tau	0.15
AB Aur	0.54
BF Ori	5.16
BD+40 4124	0.06
HD 163296	0.26

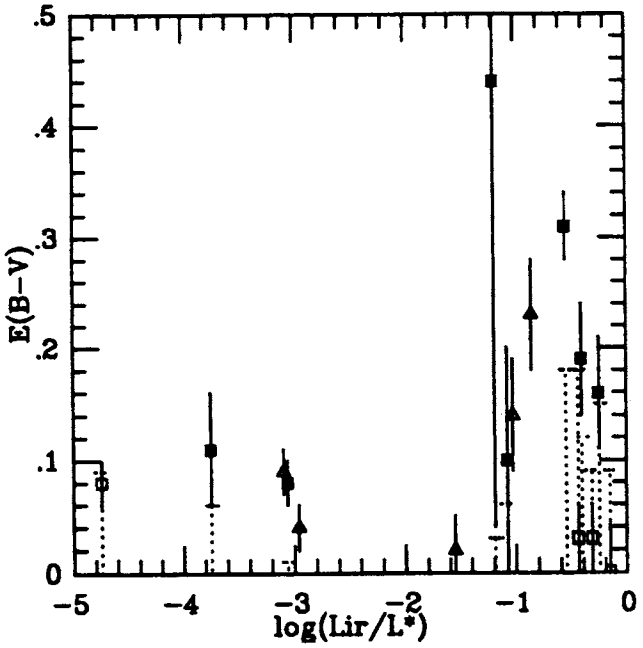

Figure 6. Plot of reddening, $E(B-V)$, versus fractional excess luminosity, L_{IR}/L_*. Triangles: stars within 10° of the Galactic plane; open squares: stars for which the Burstein & Heiles (1982) interstellar reddening in their direction is greater than the observed reddening; filled squares: stars reddened by more than the Burstein & Heiles value. Errorbars are due to uncertainties in the intrinsic colours; the Burstein & Heiles values are indicated by the dashed lines. Some points have been displaced slightly along the abscissa for clarity.

of our Vega-like stars are similar to those of Herbig Ae/Be and T Tauri stars, lending further weight to the suggestion that Vega-like stars are related to these pre-main-sequence objects.

There has been considerable debate over whether the dust around Herbig Ae/Be stars is principally in discs or envelopes (e.g. Hillenbrand et al. 1992). The rather low spectral indices at long wavelengths in our Vega-like stars may be difficult to reconcile with spherical envelopes, which naturally produce higher spectral indices than discs, but spherical envelopes should certainly be considered as a possibility for some of these sources until radiative-transfer models with appropriate geometries have been fully explored.

Alternatively, accretion luminosity is known to be a significant source of IR excess emission in the classical, strong emission line T Tauri systems (Adams et al. 1988; Calvet et al. 1994), and it seems likely that the same process may contribute to the IR excesses observed in some of our Vega-like stars too; if true, then this would further emphasize their youth and their connections with the better known pre-main-sequence stars. In order to explain the emission from the Vega-like stars with the largest IR excesses, it may therefore be necessary to consider accretion luminosity as well as the thermal reprocessing of radiation in a dust disc, if a spherical envelope does not exist.

Fig. 6 shows the reddening, $E(B-V)$, towards the stars in our sample plotted against the fractional luminosity. If the reddening were entirely due to a circumstellar dust disc, one would expect the maximum observed reddening for a given fractional luminosity to increase with L_{IR}/L_*. The distribution of points in Fig. 6 is suggestive of this, but far from compelling. Also plotted on Fig. 6 are estimates of the total *interstellar* reddening in the directions towards and beyond 11 of our sources, taken from the Burstein & Heiles (1982) maps based on HI column density, which cover Galactic latitudes $|b| > 10°$. SAO 111388 and 158350 are not included in the figure because of their highly uncertain reddenings. For four of our sources, the total interstellar reddening predicted for their directions is greater than the observed reddening towards the star, suggesting that the reddening is probably interstellar in origin. For the other seven, given the uncertainties in the intrinsic colours of the stars, and the likely inhomogeneity of the ISM, the observed reddening is reasonably consistent with the Burstein & Heiles estimates. For all of our sources, then, it appears that most or all of the reddening could plausibly be ascribed to interstellar, rather than circumstellar, dust.

Nevertheless, for a randomly oriented sample of star–disc systems, one would expect that in some cases the line of sight to the star would pass through the disc. For a flared disc with an opening angle of 10° (a rather conservative estimate), approximately 10 per cent of the stars should be seen through their discs. One might therefore expect that at least one of the stars in Fig. 6 should be seen in such a configuration, and therefore should suffer some amount of circumstellar extinction. However, circumstellar extinction could be difficult to detect, since the grain-size distribution in the dust discs is likely to contain a greater fraction of large grains than does interstellar dust, in order to produce the strong mm-wave emission observed in many of our sources (Table 14). Such a distribution would give rise to 'grey' extinction, with little reddening, even for a quite substantial total extinction. To detect grey extinction would require independent determinations of the distances and luminosities of the stars by, for example, trigonometric parallax and accurate two-dimensional spectral classification.

6 CONCLUSIONS

We have presented a variety of observational data covering the optical to mm-wave region of a sample of Vega-like stars. Most of these stars have rather larger IR excesses than the 'classical' Vega-like stars, but they still appear by and large to have relatively little reddening in the optical, which is consistent

with a disc origin for the excess emission. In a few cases the IR excess is too large to be explained entirely by reprocessing in an optically thin or thick disc, but instead requires the addition of either an envelope entirely surrounding the star (as has been proposed sometimes for Herbig Ae/Be stars) or accretion luminosity. The dust features we have observed in our mid-IR spectra reveal the presence of relatively small grains in the discs, while the very low spectral indices determined in the far-IR to mm wavebands simultaneously require the presence of very large grains, perhaps as large as a millimetre. Mid-IR spectra show silicate dust features, and the UIR bands, which produce emission features at $\lambda = 11.3$ μm and at about 7.7 μm.

ACKNOWLEDGMENTS

We are grateful to Ian Howarth for generously obtaining submm/mm-wavelength photometry of some of our sources at the JCMT. Many staff at the JCMT, UKIRT and the JKT are responsible for the successful observations of our list of sources over nearly four decades in wavelength, and we are grateful to them all. This work was supported in part (CJS) under the auspices of the US Dept of Energy under Contract No. W-7405-ENG-48 to the Lawrence Livermore National Laboratory at the Institute of Geophysics & Planetary Physics. The Jacobus Kapteyn Telescope is part of the Isaac Newton Group of Telescopes at the Observatorio del Roque de los Muchachos del Instituto de Astrofísica de Canarias, and is operated by the Royal Observatories on behalf of the Particle Physics and Astronomy Research Council of the United Kingdom and the Netherlands Organization for Scientific Research. The United Kingdom Infrared Telescope (Mauna Kea, Hawaii) is operated by the Royal Observatories on behalf of the Particle Physics and Astronomy Research Council of the United Kingdom. The James Clerk Maxwell Telescope (Mauna Kea, Hawaii) is operated by the Royal Observatories on behalf of the Particle Physics and Astronomy Research Council of the United Kingdom, the Netherlands Organization for Scientific Research and the National Research Council of Canada. IRAF is distributed by the National Optical Astronomy Observatories, which is operated by the Association of Universities for Research in Astronomy, Inc., under contract to the National Science Foundation.

REFERENCES

Adams F.C., Lada C.J., Shu F.H., 1988, ApJ, 326, 865
Aitken D.K., Moore T.J.T., Roche P.F., Smith C.H., Wright C.M., 1993, MNRAS, 265, L41
Allamandola L.J., Tielens A.G.G.M., Barker J.R., 1985, ApJ, 290, L25
Andrillat Y., Jaschek M., Jaschek C., 1990, A&A, 233, 474
Argyle R.W., Mayer C.J., Pike C.D., Jorden P.R., 1988, A User Guide to the JKT CCD Camera. Isaac Newton Group User Manual No. XVIII
Artymowicz P., Burrows C., Paresce F., 1989, ApJ, 337, 494
Aumann H.H., 1985, PASP, 97, 885
Aumann H.H. et al., 1984, ApJ, 278, L23
Backman D.E., Paresce F., 1993, in Levy E.H., Lunine J.I., eds, Protostars & Planets III. U. of Arizona, Tucson, p. 1253
Becklin E.E., Zuckerman B., 1990, in Watt G.D., Webster A.S., eds, Submillimetre Astronomy. Kluwer, Dordrecht, p. 147
Bockelée-Morvan D., André P., Colom P., Colas F., Crovisier J., Despois D., Jorda L., 1995, in Ferlet R., Vidal-Madjar A., eds, Circumstellar Dust Discs and Planet Formation. Editions Frontières, Gif sur Yvette, p. 341
Bohren C.F., Huffman D.R., 1983, Absorption and Scattering of Light by Small Particles. Wiley, New York
Burstein D., Heiles C., 1982, AJ, 87, 1165
Calvet N., Hartmann L., Kenyon S.J., Whitney B.A., 1994, ApJ, 434, 330
Chini R., Krügel E., Kreysa E., 1990, A&A, 277, L5
Chini R., Krügel E., Shustov B., Tutukov A., Kreysa E., 1991, A&A, 252, 220
Chini R., Krügel E., Kreysa E., Zylka R., 1994, Nat, 369, 714
Cohen M., Emerson J.P., Beichman C.A., 1989, ApJ, 339, 455
Cohen M., Walker R.G., Barlow M.J., Deacon J.R., 1992a, AJ, 104, 1650
Cohen M., Walker R.G., Witteborn F.C., 1992b, AJ, 104, 2030
Coulson I.M., Walther D.M., 1995, MNRAS, 274, 977
Cowley A., Cowley C., Jaschek M., Jaschek C., 1969, AJ, 74, 375
Crawford D.L., Barnes J.V., Golson J.C., 1971, AJ, 76, 1058
Deacon J.R., 1991, PhD thesis, University of London
Duley W.W., Williams D.A., 1981, Interstellar Chemistry. Academic Press, London
Duncan W.D., Robson E.I., Ade P.A.R., Griffin M.J., Sandell G., 1990, MNRAS, 243, 126
Fajardo-Acosta S.B., Telesco C.M., Knacke R.F., 1993, ApJ, 417, L33
Finkenzeller U., Mundt R., 1984, A&AS, 55, 109
Garcia-Lario P., Manchado A., Pottasch S.R., Suso J., Olling R., 1990, A&AS, 82, 497
Gillett F.C., 1986, in Israel F.P., ed., Light on Dark Matter. Reidel, Dordrecht, p. 61
Gilman R.C., 1969, ApJ, 155, L185
Gliese W., 1969, Catalogue of Nearby Stars. Publ. Astron. Rechen-Instit., Heidelb., No. 27
Golimowski D.A., Durrance S.T., Clampin M., 1993, ApJ, 411, L41
Gregorio-Hetem J., Lepine J.R.D., Quast G.R., Torres C.A.O., de la Reza R., 1992, AJ, 103, 549
Hillenbrand L.A., Strom S.E., Vrba F.J., Keene J., 1992, ApJ, 397, 613
Houk N., 1978, Michigan Catalogue of Two-Dimensional Spectral Types for the HD Stars Vol. 2. Univ. of Michigan, Ann Arbor
Houk N., 1982, Michigan Catalogue of Two-Dimensional Spectral Types for the HD Stars Vol. 3. Univ. of Michigan, Ann Arbor
Houk N., 1988, Michigan Catalogue of Two-Dimensional Spectral Types for the HD Stars Vol. 4. Univ. of Michigan, Ann Arbor
Howarth I.D., 1983, MNRAS, 203, 301
Infrared Astronomical Satellite (*IRAS*) Catalogs and Atlases, Vol. 1, Explanatory Supplement, 1988, Beichman C.A., Neugebauer G., Habing H.J., Clegg P.E., Chester T.J., eds. US Government Printing Office, Washington, DC
Johnson H.L., Mitchell R.I., Iriarte B., Wisniewski W.Z., 1966, Commun. Lunar Planetary Lab., 63, 99
Kenyon S.J., Hartmann L., 1987, ApJ, 323, 714
Knacke R.F., Fajardo-Acosta S.B., Telesco C.M., Hackwell J.A., Lynch D.K., Russell R.W., 1993, ApJ, 418, 440
Kurucz R.L., 1991, in Davis Philip A.G., Upgren A.R., Janes K.A., eds, Precision Photometry: Astrophysics of the Galaxy. L. Davis Press, Schenectady, p. 27
Lada C.J., Adams F.C., 1992, ApJ, 393, 278
Landolt A.U., 1983, AJ, 88, 439
Landolt A.U., 1992, AJ, 104, 340
Léger A., Puget J.L., 1984, A&A, 137, L5
Lesh J.R., 1968, ApJS, 17, 371
Lindroos K.P., 1985, A&AS, 51, 161
Mannings V., 1994, MNRAS, 271, 587
Matthews H.E., 1993, JCMT Manual: Part 3 – Continuum Photometry. Joint Astronomy Centre, Hilo
McLean I.S., Chuter T.C., McCaughrean M.J., Rayner J.T., 1986, in Crawford D.L., ed., Proc. SPIE Vol. 627, Instrumentation in As-

tronomy VI. SPIE, Bellingham, p. 430
Mermilliod J.P., 1986, UBV Catalogue. Centre de Données Stellaires, Strasbourg
Murphy R.E., 1969, AJ, 74, 1082
Neugebauer G. et al., 1986, A&AS, 65, 607
Pollack J.B., Hollenbach D., Beckwith S., Simonelli S.B., Roush T., Fong W., 1994, ApJ, 421, 615
Rydgren A.E., Schmelz J.T., Zak D.S., Vrba F.J., 1984, Publ. US Naval Observatory, 25, 1
Sadakane K., Nishida M., 1986, PASP, 98, 689
Sandell G., 1994, MNRAS, 271, 75
Schmidt-Kaler Th., 1982, in Schaifers K., Voigt H.H., eds, Landolt-Börnstein, Numerical Data and Functional Relationships in Science and Technology, Group VI, Astronomy, Astrophysics and Space Research, Vol. 2b. Springer-Verlag, Berlin, p. 14
Seaton M.J., 1979, MNRAS, 187, 73P
Sellgren K., Werner M.W., Dinerstein H.L., 1983, ApJ, 217, L149
Shu F.H., Adams F.C., Lizano S., 1987, ARA&A, 25, 23
Skinner C.J., Whitmore B., 1988, MNRAS, 235, 603
Skinner C.J., Barlow M.J., Justtanont K., 1992, MNRAS, 255, 31P
Skinner C.J., Sylvester R.J., Graham J.R., Barlow M.J., Meixner M., Keto E., Arens J.F., Jernigan J.G., 1995, ApJ, 444, 861
Smith B.A., Terrile R.J., 1984, Sci, 226, 1421
Stencel R.E., Backman D.E., 1991, ApJS, 75, 905
Stern S.A., Festou M.C., Weintraub D., 1994a, Nat, 368, 312
Stern S.A., Festou M.C., Weintraub D., 1994b, Nat, 369, 766
Stevens J.A., Robson E.I., 1994, MNRAS, 270, L75
Sylvester R.J., Barlow M.J., Skinner C.J., 1992, in Gondhalekar P.M., ed., Proc. Workshop on Astronomy and Astrophysics, Dusty Discs. RAL Report 92-084, p. 172
Sylvester R.J., Barlow M.J., Skinner C.J., 1994a, MNRAS, 266, 640
Sylvester R.J., Barlow M.J., Skinner C.J., 1994b, Ap&SS, 212, 261
Sylvester R.J., Barlow M.J., Skinner C.J., 1996, ApJ, submitted
Telesco C.M., Knacke R.F., 1991, ApJ, 372, L29
Turon C. et al., 1992, The Hipparcos Input Catalogue. ESA SP-1136
Upgren A.R., Grossenbacher R., Penhallow W.S., 1972, AJ, 77, 486
van der Veen W.E.C.J., Habing H.J., Geballe T.R., 1989, A&A, 226, 108
van der Veen W.E.C.J., Waters L.B.F.M., Trams N.R., Matthews H.E., 1994, A&A, 285, 551
Walker H., Wolstencroft R.D., 1988, PASP, 100, 1509 (WW)
Walter F.M., Brown A., Mathieu R.D., Myers P.C., Vrba F.J., 1988, AJ, 96, 297
Waters L.B.F.M., Coté J., Geballe T.R., 1988, A&A, 203, 348
Weintraub D.A., Stern S.A., 1994, AJ, 108, 701
Welty D.E., Hobbs L.M., Blitz L., Penprase B.E., 1989, ApJ, 346, 232
Whitmire D.P., Matese J.J., Whitman P.G., 1992, ApJ, 388, 190
Woolf N.J., Ney G.P., 1969, ApJ, 155, L181
Zuckerman B., Becklin E.E., 1993, ApJ, 414, 793
Zuckerman B., Forveille T., Kastner J.H., 1995, Nat, 373, 494

This paper has been produced using the Royal Astronomical Society/Blackwell Science LaTeX style file.